land

MDPI

Article

Field-Scale Winter Wheat Growth Prediction Applying Machine Learning Methods with Unmanned Aerial Vehicle Imagery and Soil Properties

Lwandile Nduku [1,2,*], Cilence Munghemezulu [2], Zinhle Mashaba-Munghemezulu [2], Wonga Masiza [2], Phathutshedzo Eugene Ratshiedana [2], Ahmed Mukalazi Kalumba [3] and Johannes George Chirima [1,2]

[1] Department of Geography, Geoinformatics & Meteorology, University of Pretoria, Pretoria 0028, South Africa
[2] Geoinformation Science Division, Agricultural Research Council, Institute for Soil, Natural Resources and Engineering, Pretoria 0001, South Africa; MunghemezuluC@arc.agric.za (C.M.); MasizaW@arc.agric.za (W.M.); ratshiedanap@arc.agric.za (P.E.R.)
[3] GACCES Lab, Department of Geography & Environmental Science, University of Fort Hare, Alice 5700, South Africa; akalumba@ufh.ac.za
* Correspondence: ndukulwandile@gmail.com

Abstract: Monitoring crop growth conditions during the growing season provides information on available soil nutrients and crop health status, which are important for agricultural management practices. Crop growth frequently varies due to site-specific climate and farm management practices. These variations might arise from sub-field-scale heterogeneities in soil composition, moisture levels, sunlight, and diseases. Therefore, soil properties and crop biophysical data are useful to predict field-scale crop development. This study investigates soil data and spectral indices derived from multispectral Unmanned Aerial Vehicle (UAV) imagery to predict crop height at two winter wheat farms. The datasets were investigated using Gaussian Process Regression (GPR), Ensemble Regression (ER), Decision tree (DT), and Support Vector Machine (SVM) machine learning regression algorithms. The findings showed that GPR (R^2 = 0.69 to 0.74, RMSE = 15.95 to 17.91 cm) has superior accuracy in all models when using vegetation indices (VIs) to predict crop growth for both wheat farms. Furthermore, the variable importance generated using the GRP model showed that the RedEdge Normalized Difference Vegetation Index (RENDVI) had the most influence in predicting wheat crop height compared to the other predictor variables. The clay, calcium (Ca), magnesium (Mg), and potassium (K) soil properties have a moderate positive correlation with crop height. The findings from this study showed that the integration of vegetation indices and soil properties predicts crop height accurately. However, using the vegetation indices independently was more accurate at predicting crop height. The outcomes from this study are beneficial for improving agronomic management within the season based on crop height trends. Hence, farmers can focus on using cost-effective VIs for monitoring particular areas experiencing crop stress.

Keywords: winter wheat; crop growth; vegetation indices; soil properties; machine learning

Citation: Nduku, L.; Munghemezulu, C.; Mashaba-Munghemezulu, Z.; Masiza, W.; Ratshiedana, P.E.; Kalumba, A.M.; Chirima, J.G. Field-Scale Winter Wheat Growth Prediction Applying Machine Learning Methods with Unmanned Aerial Vehicle Imagery and Soil Properties. *Land* **2024**, *13*, 299. https://doi.org/10.3390/land13030299

Academic Editor: Paul Aplin

Received: 19 December 2023
Revised: 21 February 2024
Accepted: 22 February 2024
Published: 27 February 2024

1. Introduction

Wheat is one of the most widely grown cereal crops, covering about 220.62 million hectares (ha) worldwide in 2022/23 [1–3]. During this period, the yield increased steadily, providing about 789.02 million metric tons globally [4]. Wheat provides between 20% and 36% of calories for the world's population [5,6]. The Food and Agriculture Organization (FAO) emphasises that the rapidly growing population and escalating demands for cereal production would require a 70% increase in cereal supply by 2050 [1,7,8]. Monitoring wheat growth is essential for meeting future food demands and ensuring food security, which promotes sustainable agricultural management and enhances yields. However, variations in soil properties, agro-ecosystems, topography, and crop growth conditions within fields

impact crop growth [1,7]. Furthermore, wheat growth is affected by variations in the intra-field soil properties; biological, physical, and chemical factors; and management practices [7]. Accurate in situ measurements and establishing the distribution of soil properties within planted areas are crucial for understanding their impact on intra-field crop growth and promoting sustainable agricultural management [9–11].

Soil physical and chemical properties regulate soil productivity, which influences crop development [12]. Concurrently, infertile acidic soils are detrimental to crop development. Infertile soils are characterised by high aluminium (Al) toxicity, low pH (acidic), low microbial activity, low soil organic carbon, and a lack of essential chemical properties that hinder wheat growth at the early development stages [5,13]. These soil conditions and characteristics result in problems such as reduced root branching, deformed root tips, lodging, and the discolouration of leaf tissue with shades of yellow and purple [13,14]. Furthermore, wheat cultivated within infertile acidic soil experiences a reduced protein content and growth rate and lower yields, which result in reduced profits. Soil elements such as phosphorus (P), potassium (K), magnesium (Mg), calcium (Ca), sodium (Na), nitrogen (N), and pH are vital for crop growth and often exist in low concentrations in arid and semi-arid environments [15–18]. Deficiencies of N, P, and K in soil affect wheat growth and yield drastically [19]. The influence of intra-field soil physiochemical properties' variation and meteorological conditions are key factors on crop development across various crop stages. Other detrimental effects on wheat growth include abiotic stresses such as droughts, frost, waterlogging, salinity, high temperatures, and other natural calamities [20,21]. The biotic factors, which include the infestation of diseases, competing weeds, and pests, are common challenges for crop development [22–25].

There are various vegetation indices derived from the red and near-infrared (NIR) bands, which aid in the understanding of vegetation absorption and reflectance properties. These vegetation indices are commonly used in monitoring crop development, growth, and associated stresses during various phenological stages of the crop for timely interventions in farm management [26–28]. In addition to vegetation indices derived from satellite products, UAV-derived indices can also aid in detecting the intra-field spatial variability of wheat crop growth with a higher spatial resolution and accuracy compared to most satellite products. The existing conventional methods (i.e., scouting and automated observation systems using computer vision) to monitor crop growth variation do not accommodate vegetation indices to model and predict intra-field crop growth. Furthermore, traditional methods are time-consuming, labour-intensive, and unrealistic for time-series modelling required by large-scale farms. They usually result in many forms of inaccuracies associated with human survey errors [29]. Recent developments of UAVs in remote sensing provide an efficient, non-destructive, and rapid alternative approach that can provide cost-effective time-series data of vegetation indices for modelling crop growth variability [29,30]. However, the reflectance can be greatly affected by the surface temperature, atmospheric distortions, water content, saturation, landscape heterogeneity, and vegetation type, which can affect the modelling accuracies of actual crop growth [27,31]. Moreover, coarse spatial resolution satellite imagery limits the regression model estimation accuracy due to spectral mixing of different classes [32]. Combining high-resolution UAV-derived vegetation indices with in situ soil properties' data can enhance crop growth modelling. For example, a Belgian case study confirmed that soil properties account for 15 to 26% of the wheat growth variance using machine learning methods with UAV imagery [7]. A case study of Southwest Montana in the USA has successfully predicted accurate soil properties and wheat growth variation using machine learning algorithms and vegetation indices derived from UAV imagery [13]. The integration of UAV-based imagery and elevation data improved modelling accuracies based on machine learning methods for wheat height growth and above-ground biomass in Fengling Reservoir fields in China [33]. Nevertheless, there is still a lack of methods, which integrate the multiple factors influencing plant growth as well as quantifying their importance in modelling.

The common modelling approaches include parametric and non-parametric regression for crop biophysical parameter estimation. These include partial least squares regression (PLSR), random forest (RF), support vector machine (SVM), extreme gradient boosting (Xgboost), conditional inference forest (CI-forest), artificial neural network (ANN), least squares linear regression (LSLR), multiple linear regression (LR), neural network (NN), decision tree (DT), regression tree (RegT), K-nearest neighbour (KNN), boost tree (BST), and bagging tree (BagT) ensemble learning algorithms [7,18,30,34–36]. PLSR provides a high level of interpretability and can overcome problems of collinearity in modelling, enhancing the accuracy of the model [9,17]. However, other studies suggest that PLSR is not always adequate for modelling the relationship between soil properties and crop height because this relationship is not always linear [37–39]. This limitation has contributed to the rising need for exploring the use of nonlinear machine learning algorithm (MLA) methods and other models. RF has the capabilities to classify and handle complex data with continuous values, but it is not robust and sensitive to outliers, which can cause overfitting or poor generalisation, and it does not address collinearity when applied with large or small input data [40–42]. SVM has similar merits and demerits to RF, except that it uses kernel-based functions for mapping input features at higher dimensional space and exploits support vectors for fixing regression fitting [43]. In general, several MLAs such as NNs, RF, SVM, KNN, RegT, and Xgboost often experience black box problems, among others [44–46]. Meanwhile, GPR has the capability of overcoming the black box challenges by employing kernel functions, which offer uncertainty estimates for model predictions across a spectrum of data inputs, ranging from simple to highly complex [45,46]. Kernel-based regression algorithms such as GPR are superior to several MLAs in retrieving modelling accuracy [47,48]. Few studies have reported the feasibility of kernel-based methods in modelling wheat biophysical variables such as crop height using time-series vegetation indices' data for an entire season [49]. A multispectral sentinel-2 dataset has shown a potential estimation of crop biophysical variables such as the plant height, leaf area index (LAI), leaf chlorophyll content (LCC), fraction of absorbed photosynthetically active radiation (FAPAR), fraction of vegetation cover (FVC), and canopy chlorophyll content (CCC) using random forest tree bagger (RFTB), BagT, LSLR, PLSR, and GPR [46,49–51]. However, studies focusing on soil properties and UAV datasets that have a high spatial, spectral, and temporal resolution are lacking. UAVs have a high potential for estimating field-scale wheat growth.

This study addresses a gap in the existing literature by focusing on the integration of high-resolution UAV-derived vegetation indices with in situ soil properties' measurements [7,13]. This could contribute to a more comprehensive understanding of the factors influencing wheat growth and enhance the modelling accuracy. Furthermore, this study aims to investigate machine learning regressions such as GPR, ER, DT, and SVM for predicting wheat crop height using a combination of UAV-derived vegetation indices and soil properties. By considering multiple factors simultaneously, the research aims to fill a gap related to the absence of holistic approaches in previous studies that often focused on individual aspects of wheat growth. Additionally, while previous studies have explored UAV imagery and soil properties, this study specifically aims to address the gap in research focusing on field-scale wheat growth variability [7,14,35]. This may involve considering the spatial, spectral, and temporal resolution of data to provide more detailed insights into wheat height variability patterns. The main objectives of this study were to (1) investigate and understand the contribution of soil properties and vegetation indices in modelling crop height of heterogeneous winter wheat planted in a dryland environment, and (2) assess the prediction accuracy changes when using the vegetation-index-only scenario and combined vegetation indices with soil properties scenario for wheat crop height. Although experiments were conducted in South Africa, the techniques developed in this study can be tested in other semi-arid regions as well. An example is Australia, which is a major producer of wheat and is also facing a decline in wheat production [52]. India is also a significant wheat-producing country with diverse agro-climatic zones and unique

challenges related to smallholder farming, decreasing soil nutrients, and issues in water resource management [53].

2. Materials and Methods

Figure 1 provides an overview of the methodology used in this study to investigate the contribution of vegetation indices and soil physical and chemical properties to wheat crop height. The physical and chemical properties of the soil samples were used for generating kriging spatial interpolation maps. UAV data bands were used to calculate the vegetation indices' map. The vegetation indices' data were first used separately and secondly stacked with kriging soil properties for model prediction. The datasets were divided into 80% for the training set and 20% for the testing set for GRP, ER, DT, and SVM models. Thereafter, model evaluation accuracy was generated for all the evaluated models.

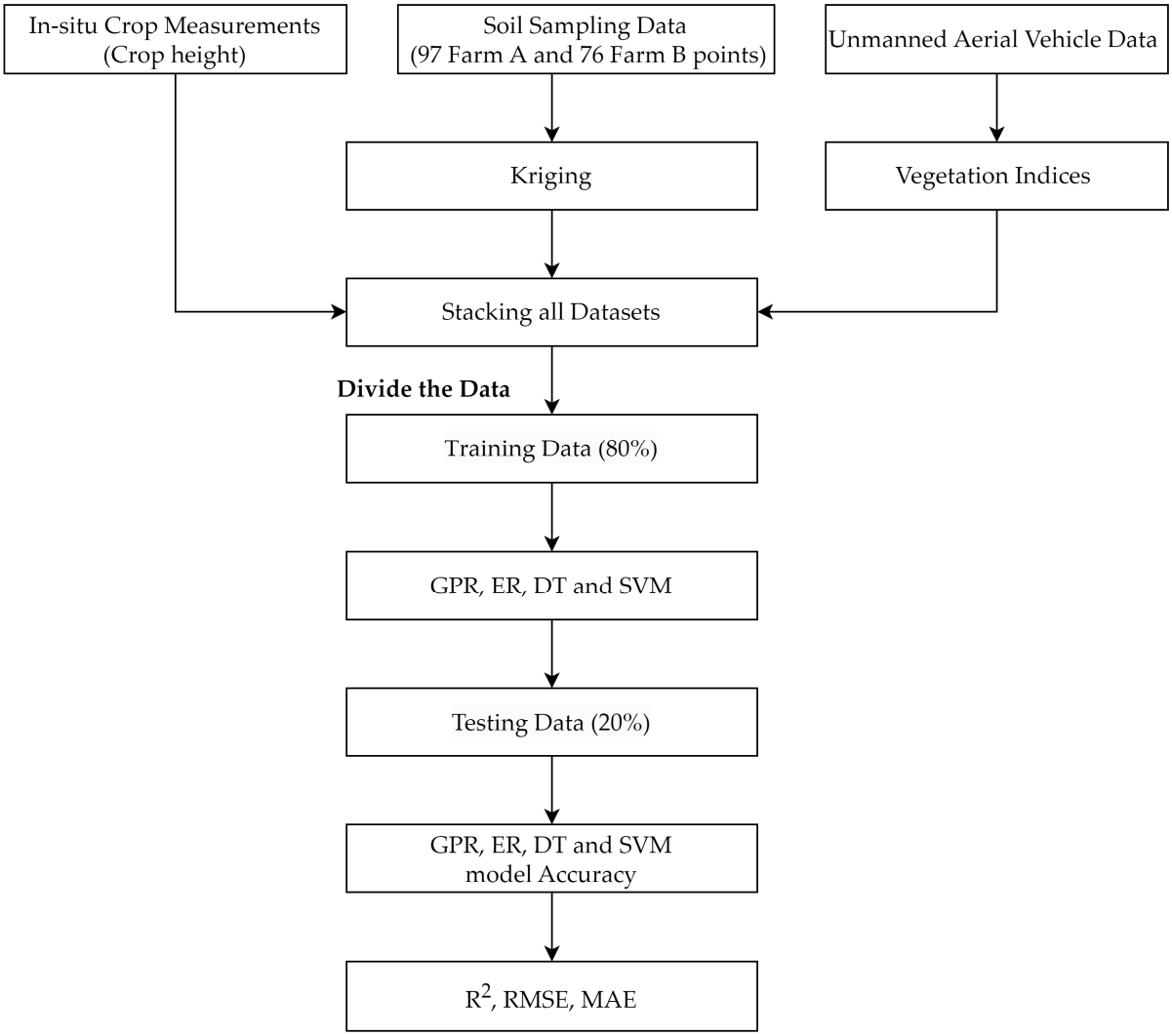

Figure 1. Methodology flowchart for intra-field crop growth modelling used in this study.

2.1. Study Area

The Clarens experiment wheat farms cover about 30 ha (Farm A) and 17 ha (Farm B). The two farms were prepared using Cireun 100 kg/ha fertilizer with a ratio of N:55:P:15:K:8 for cultivar PAN: 3161. This wheat cultivar is suitable for sowing in the dryland production areas of the Free State province. The two farms are located at the Dihlabeng Local Municipality (DLM) within the Thabo Mofutsanyane district in the northern part of the Free State province in South Africa (Figure 2). The municipality receives an annual average rainfall of 688 mm, a minimum of 7.8 °C in the summer season, and a maximum of 20.7 °C (average

temperatures) during the winter and summer season [54]. Most rainfalls occur in summer with hot days and cold dry winter seasons [55,56]. The predominant soil type is sandy loam with Avalon and Pinedene characteristics that indicate moderately permeable soils [57]. The Thabo Mofutsanyane district is characterised by dryland production areas and is one of the main rainfed winter wheat producers in the Free State province [58,59]. However, long dry spells, droughts, and frost occurrence are prominent climatic drivers that affect crop yields and agricultural production in this region [60–63]. The reliance of winter wheat on rainfall in the Free State province makes it susceptible to the risk of altered rainfall distribution patterns and declining rainfall amounts, which affect the rate of growth and anticipated yields [61–63]. The selected case study locations cultivate wheat consistently. Nevertheless, the farmers have been experiencing declining yields in recent years, which could be linked to several factors such as soil properties' variability and changing climate conditions that cause crop stress. A previous study based on this region only focused on the characterisation of wheat nematodes from cultivars [58]. There is currently a lack of studies that focus on the biophysical properties of both soil and crops.

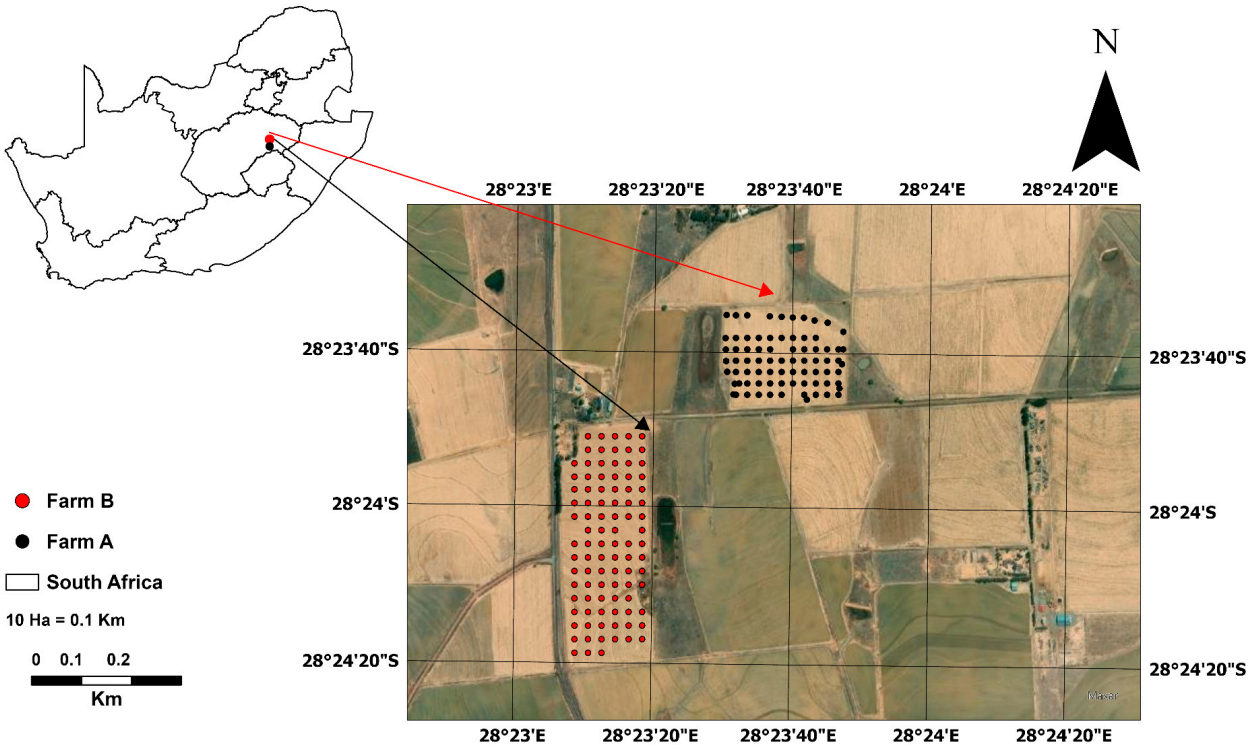

Figure 2. Map showing the location of the Clarence wheat farms in the Thabo Mofutsanyane district in the Free State province of South Africa.

Figure 3 displays the monthly rainfall and temperatures received by Clarens wheat farms throughout 2021. The rainfall and temperatures were downloaded from NASA POWER (https://power.larc.nasa.gov/, accessed on 12 January 2024). NASA POWER has a spatial resolution of 0.5° latitude by 0.5° longitude to provide daily temperatures at 2 m and precipitation (mm/day) among other climate variables [64]. Despite the low rainfall amount and relatively moderate temperatures received during wheat-growing months, an upward trend in average temperatures and rainfall was recorded between August and November 2021.

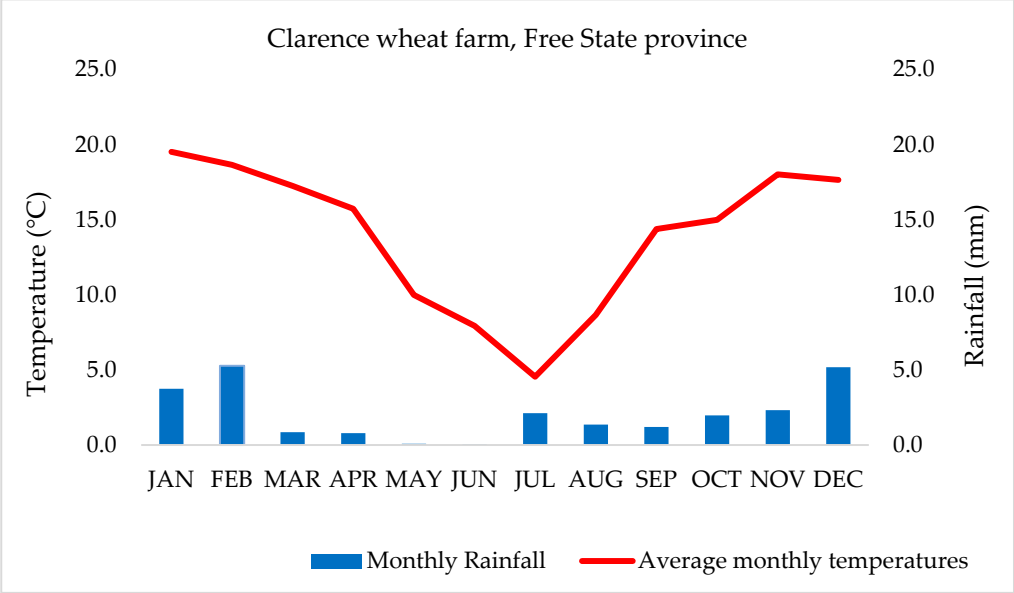

Figure 3. Average monthly meteorological rainfall and temperature data from January to December 2021.

2.2. Field Data Collection

2.2.1. Analytical Analysis of Soil Samples

The soil samples collected amounted to 97 (Farm A) and 76 (Farm B) collected within a 0–20 cm depth in the topsoil layer, during the dry month of August 2021. A handheld Global Positioning System (GPS) was used to capture the spatial position of each sampled point. All the soil-sample-processing procedures were administered by the Agricultural Research Council Institute for Soil, Climate and Water Analytical Laboratory. These procedures include air-drying the soil samples at 25 °C and crushing and sieving them into a less than 2 mm size to remove gravel stones and plant residues. All soil samples were mostly characterised by sandy loam and clay soil textures. Multiple analytical processing methods were used to classify soil physical properties, chemical nutrients, and texture (as described in Table 1 below).

Table 1. Summary of analytical soil physical and chemical properties.

Soil Physical Properties and Chemical Nutrients	Analytical Processing Methods	References
P	Bray-1 method	[65,66]
K, Ca, Na, Mg	Ammonium acetate method	[67,68]
pH	H_2O	[69]
Sand, Silt, Clay	Crushed and sieved (particle size < 2 mm), remove gravel stones and plant residues	[68]

2.2.2. UAV Data Collection and Crop Height Measurements

Between August and November 2021, UAV flight missions and in situ measurements were conducted during early tillering and heading stages of winter wheat growth on both farms. Table 2 displays the results. Ground crop height measurements were performed using a metal tape measure in centimetres (cm). All flight missions were planned at a 120 m height above the surface and the UAV imagery overlap was set at 75% for both frontal and lateral overlaps. Thus, a spatial resolution with a pixel size of 8 cm UAV imagery was obtained under clear sky conditions and moderate wind speeds. Figure 4a depicts the multi-rotor UAV DJI-Matrice 600 Pro system with a MicaSense RedEdge-MX multispectral sensor. Figure 4b shows the calibration reflectance panel (CPR) used to calibrate the acquired UAV tiles during data processing.

Table 2. UAV-Survey Scheduled and ground-based measurements at different winter wheat growth stages across Farm A and Farm B.

Activities	Crop Phenological Stage	Crop Height	UAV-Survey Dates
Planting	Seeding	No	2 July 2021
First flight	Tillering	Yes	17 August 2021
Second flight	Jointing	Yes	14 September 2021
Third flight	Booting	Yes	18 October 2021
Fourth flight	Flowering	Yes	15 November 2021
Fifth flight	Heading/ripening	Yes	29 November 2021

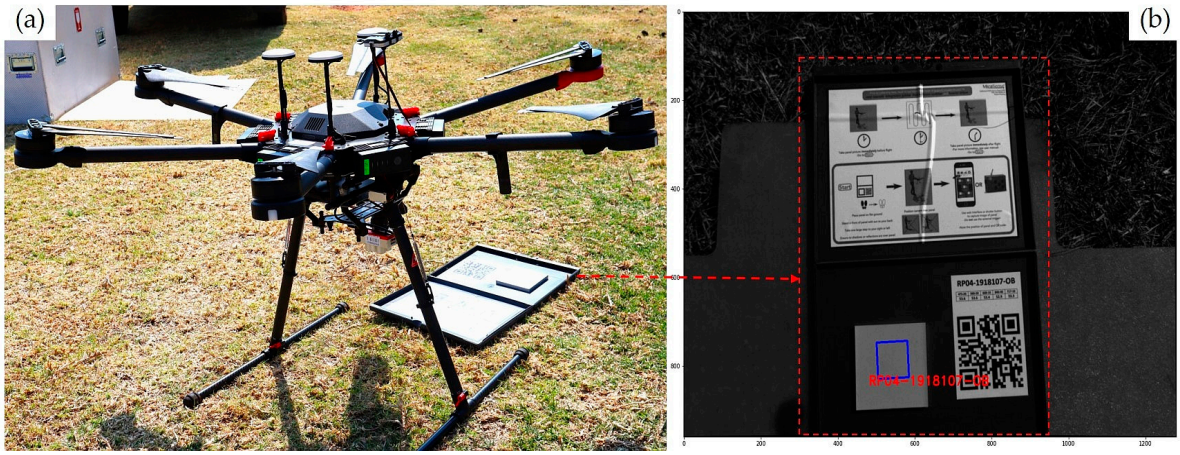

Figure 4. Multi-rotor DJI Matrice 600 Pro system equipped with MicaSense RedEdge-MX sensor (**a**) and a MicaSense Calibration Reflectance Panel serial number: RP04-1918107-OB (**b**).

The information in Table 3 presents spectral information about MicaSense RedEdge-MX camera wavelength (475–840 nm), bandwidth (20–40 nm), and constant laboratory-calibrated reflectance panel (CRP) values ranging from 0.532 to 0.536, respectively. The integration of sensor measurements' irradiance of a Downwelling Light Sensor (DLS) and CRP is vital during the calibration process to construct accurate surface reflectance in all spectral bands.

Table 3. Properties of the MicaSense RedEdge-MX series sensor.

Band Name	Centre Wavelength (nm)	Bandwidth (nm)	Calibrated Reflectance Panel
Blue	475	20	0.536
Green	560	20	0.536
Red	668	10	0.534
RedEdge	717	10	0.529
NIR	840	40	0.533

2.3. UAV Data Processing

Generally, the process of UAV image processing involves (1) aerial triangulation, (2) Digital Surface Model (DSM) generation, (3) the rectification of individual images, and (4) an orthomosaic [70]. Radiometric, geometric-corrected, vignette-corrected, and mosaicking of UAV imagery collections from different surveys on winter wheat fields were carried out using Pix4Dmapper software 4.8.0 version (Pix4D SA, Lausanne, Switzerland) to produce accurate orthorectified surface reflectance images. Before each flight, pictures from the radiometrically calibrated target, the position of the sun, and incoming radiance were simultaneously measured. The data captured are used to generate surface reflectance imagery. The UAV onboard Global Positioning System (GPS) sensor data are used in the

bundle block adjustment process by applying the Structure from Motion (SfM) algorithm to compute the relative locations of the sensors during the flight and to simultaneously calculate the sensor parameters of each image [71]. A DSM was generated using the dense point cloud by applying multi-view stereo matching [72] and grid interpolation. Orthomosaicked individual images are combined into five multispectral bands. This process was also followed by similar studies such as [73,74].

2.4. Wheat Crop Growth Band Spectral Response

The earth's surface features have different spectral reflectance (spectral signatures) in the electromagnetic spectrum [75]. Figures 5 and 6 in Farm A and Farm B (A–E) present five different spectral bands of reflectance generated after UAV processing from tillering to ripening wheat growth stages. Generally, the reflectance from the five spectral bands varied from August 2021 to November 2021. The Blue (A), Green (B), and Red (C) spectral bands were less sensitive to surface reflectance of wheat growth canopies because of chlorophyll absorption in visible light of the electromagnetic spectrum. However, the RedEdge (D) and NIR (E) spectral bands showed a substantial wheat surface reflectance variation at different stages. Overall, both RedEdge and NIR are very important spectral bands in detecting intra-season crop growth changes.

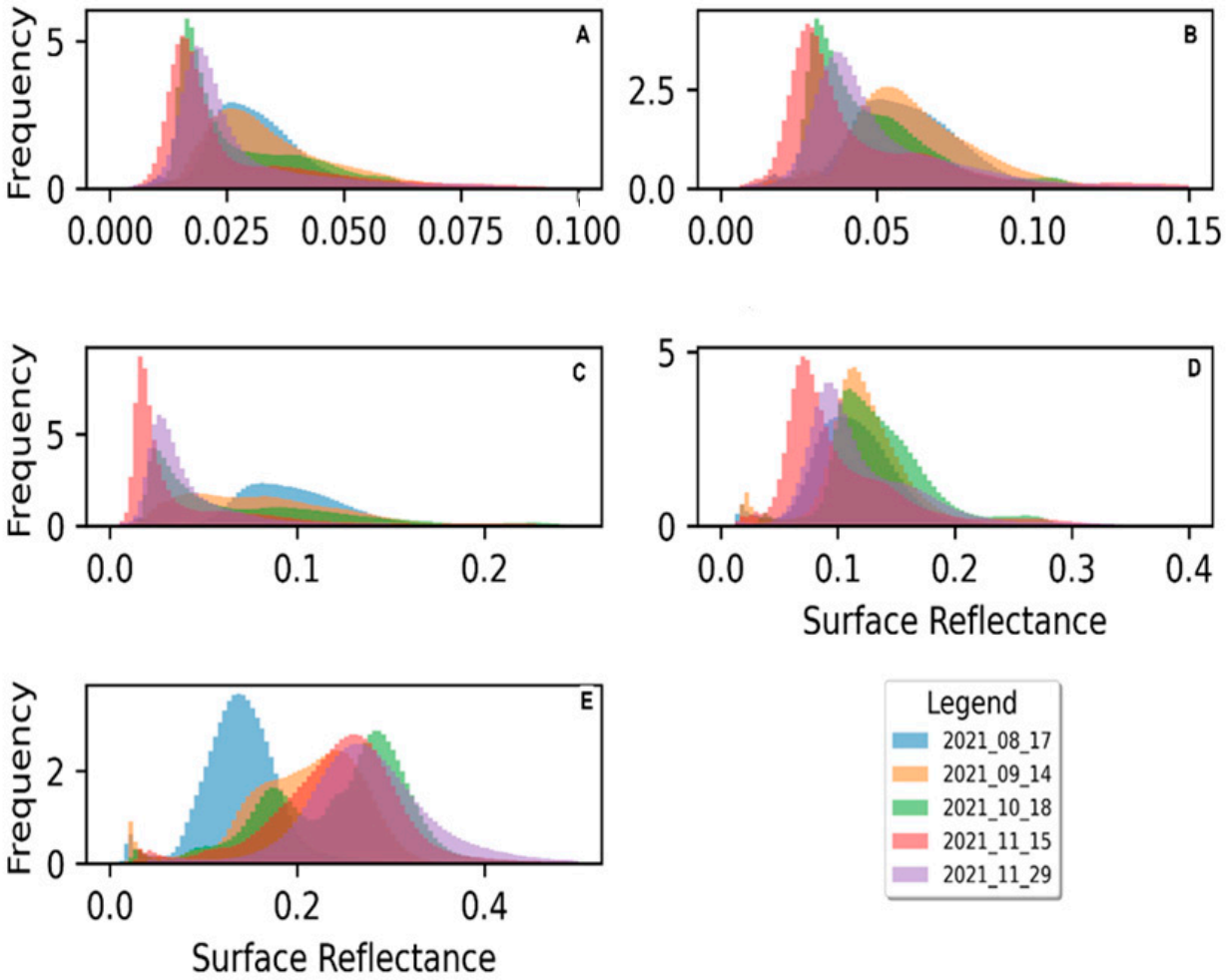

Figure 5. Farm A spectral bands' surface reflectance of wheat at different stages ((**A**) = Blue, (**B**) = Green, (**C**) = Red, (**D**) = RedEdge, (**E**) = NIR). The frequency values are scaled by 10^6.

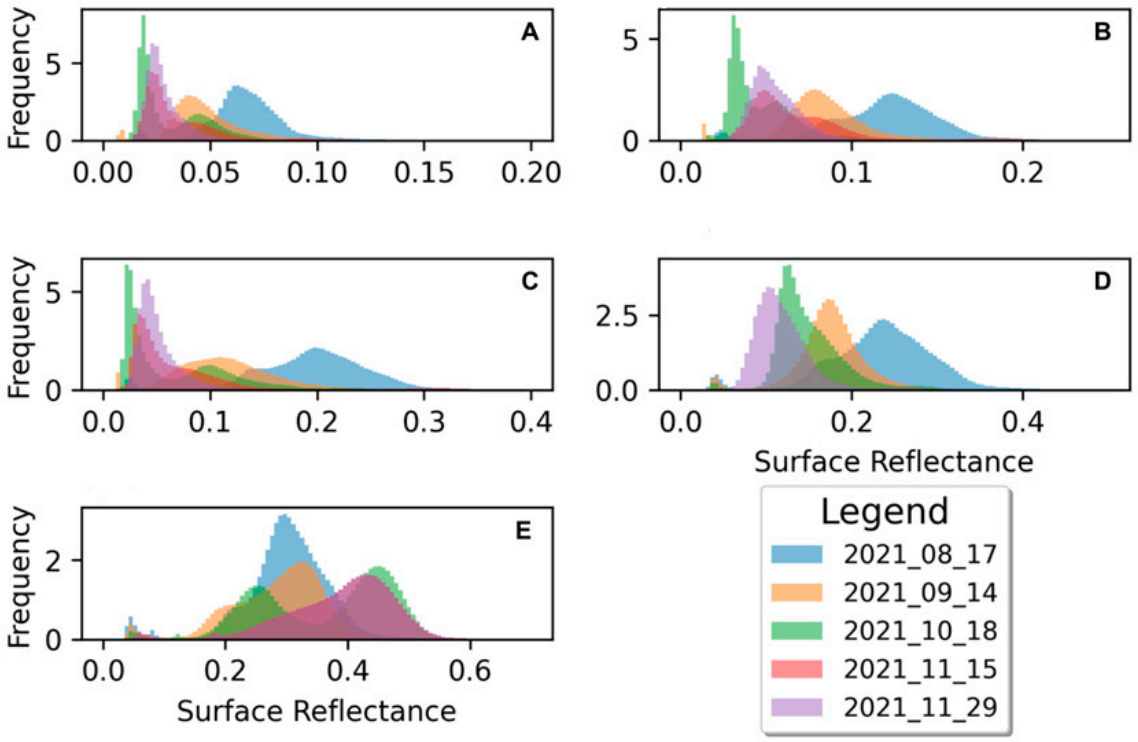

Figure 6. Farm B spectral bands' surface reflectance of wheat growth canopies at different stages ((**A**) = Blue, (**B**) = Green, (**C**) = Red, (**D**) = RedEdge, (**E**) = NIR). The frequency values are scaled by 10^6.

2.5. Derived Vegetation Spectral Indices

The list of vegetation indices in Table 4 was computed using different spectral bands from the UAV imagery. This study used the following vegetation indices: Normalized Difference Vegetation Index (NDVI), RedEdge Normalized Difference Vegetation Index (RENDVI), Normalized Difference Index (NDI), and Ratio Vegetation Index 2 (RVI 2). The selection of the above indices was based on the previous literature of similar studies that showed their capacity to characterise crop growth heterogeneity, reduce saturation, and improve model predictions [7,76].

Table 4. Vegetation spectral indices were used in this study.

Vegetation Indices	Formula (s)	Justification	Reference
NDVI	$\frac{NIR-Red}{NIR+Red}$	Common index used for leaf coverage and crop health	[77]
RENDVI	$\frac{NIR-RedEdge}{NIR+RedEdge}$	Sensitive to chlorophyll content in crop leaves against soil background effects	[7]
NDI	$\frac{RedEdge-Red}{RedEdge+Red}$	Sensitive to crop stress	[7]
RVI2	$\frac{Red}{RedEdge}$	High potential to indicate the stress level of crops	[76]

2.6. Intra-Field Crop Growth Modelling Using Different Machine Learning Regressions

In this study, the four models including GPR, ER, DT, and SVM were selected for intra-field crop growth modelling and mapping. These regression models are explained in the following sub-sections.

2.6.1. Gaussian Process Regression (GPR)

The GPR is a non-parametric kernel-based MLA, which can learn the relationship between the dependent and independent variables by fitting Bayesian statistics [78,79].

GPR generally uses simple parameter optimisation in comparison to other machine learning regression methods [80,81]. However, it can be automatically completed by maximising the marginal likelihood in the training dataset [5]. The GPR used in this study was applied in MATLAB software R2019b version.

2.6.2. Ensemble Regression (ER)

ER consists of least squares boosting trees (LSboost) and bagging trees (BGTs). Ensemble approaches construct a baseline group of learning (classifiers) procedures that are combined by voting on their estimations [81,82]. Bagging creates baseline learners by producing simulated bootstrap data and boosting the weights of the training set samples [83]. However, there are several differences in bagging and boosting learning algorithms [84]. Bagging selects the training samples randomly and autonomously while boosting has succession relation to the previous learning. Furthermore, bagging has equal weights and boosting has different weights for all base learners. Bagging generates parallel base learners and boosting chronologically. Both the bagging and boosting regression approaches often perform better than a single classifier. This occurs because of the generation of classifiers with higher accuracy through combining diverse classifiers with lower accuracy, which is often applied to learn complex and nonlinear data in solving practical problems [44]. This study applied ensemble learning algorithms using MATLAB software [83,85].

2.6.3. Decision Trees (DTs)

DT belongs to non-parametric algorithms, which are used for both regression and classification tasks [86,87]. DT is a supervised machine learning method and its principle relies on using probability trees to facilitate the decision-making process and estimate the value of a target feature. Additionally, DT is a built model to learn all the decision rules inferred from the input data variables and later can be used to make decisions and estimations. Optimisable DT uses optimal parameters and hyperparameters to create a system that can define search space for distinct hyperparameters. This study used MATLAB software to train the DT model.

2.6.4. Support Vector Machines (SVMs)

The SVM is a nonlinear and non-parametric method that relies on kernel functions (mathematical functions) [88–90]. The kernel functions transform the input data into the required format using SVM algorithms [91]. The principle of kernel functions is to help translate input data into higher-dimensional space for receiving it linearly and separately by a hyperplane in solving quadratic optimisation problems [92]. The SVM algorithms use different types of kernel functions, which consist of the radial basis function (RBF) and sigmoid, Gaussian polynomial, linear, and sinusoidal functions [93,94]. The nonlinear kernels such as RBF usually perform better than linear kernels, while the linear kernels have efficient computation [95]. To improve performance in RBF kernels, both the sigma parameter and complexity C (regularisation) parameter need to be enhanced in the prediction process [96]. Furthermore, SVM has several hyperparameters that influence its performance, such as the choice of kernel, regularisation parameter, and kernel-specific parameters. These hyperparameters need to be carefully tuned using techniques like cross-validation to obtain the best model performance [90,97]. SVM is a common regression method for modelling different crop biophysical parameters. This study applied SVM using MATLAB software.

2.6.5. Kriging

Kriging is the geostatistical algorithm that predicts the value of unsampled points using the procedure of weighing neighbouring point values [98,99]. The ordinary kriging (OK) procedure was applied to interpolate the value of unsampled points and generate maps of soil physical and chemical properties with Equation (1). The soil sampled input data were used to compute spatial variation structure and evaluated using a semi-variogram [100,101].

All OK spatial interpolation semi-variogram maps were produced based on the least RMSE on cross-validation during the selection of spherical (2), Gaussian (3), stable (4), exponential (5), and circular (6) models.

$$\hat{Z}(S_0) = \sum_{i=1}^{n} \lambda_i \, Z(S_i) \tag{1}$$

$$\gamma(h) = \begin{cases} c_o + c\left(\frac{3h}{2a} - \frac{1}{2}\left(\frac{h^3}{a^3}\right)\right) & 0 < h \le a \\ c_0 + c & h > a \\ 0 & h = 0 \end{cases} \tag{2}$$

$$\gamma(h) = \begin{cases} c_o + c\left(1 - exp\left(-\frac{h^2}{a^2}\right)\right) & h > 0 \\ 0 & h = 0 \end{cases} \tag{3}$$

$$\gamma(h) = \begin{cases} c_o + c\left(\frac{h}{a}\right) & 0 < h \le a \\ c_0 + c & h > a \\ 0 & h = 0 \end{cases} \tag{4}$$

$$\gamma(h) = \begin{cases} c_o + c\left(1 - exp\left(\frac{-h}{a}\right)\right) & h > 0 \\ 0 & h = 0 \end{cases} \tag{5}$$

$$\gamma(h) = \begin{cases} c_o + \frac{2c}{\pi}\left(\frac{h}{a}\sqrt{1 - \left(\frac{h^2}{a^2}\right)} + arcsin\left(\frac{h}{a}\right)\right) & 0 < h \le a \\ c_0 + c & h > a \\ 0 & h = 0 \end{cases} \tag{6}$$

where $Z(S_i)$ is the measured value at the ith location; λ_i is an unknown weight for the measured value at the ith location; $\hat{Z}(S_0)$ is the prediction location; n is the number of measured values separated by the distance h. The values of c_o, c, and a are derived on estimated standard error (SE) parameters fitted to semi-variograms.

2.7. Experiments

The study investigated the contribution of soil properties and vegetation indices to improve the modelling accuracy of intra-field crop growth variability for two winter wheat farms. The first experiment used vegetation-index-only datasets as predictor variables for wheat crop height (Table 5). Furthermore, the second experiment used a combination of vegetation indices and soil properties as predictor variables. The K-10-fold cross-validation was applied to divide datasets into 80% (400 points) for the training set and 20% (100 points) for the testing set for Farm A, while datasets for Farm B were split into 80% (304 points) for the training set and 20% (76 points) for the testing set. MATLAB software was used to run the four machine learning regressions consisting of GPR, ER, DT, and SVM.

Table 5. Experimental dataset for training and testing GPR, ER, DT, and SVM models.

Experiment	Number of Predictor Variables	Data Configuration
1	4	Vegetation indices
2	12	Vegetation indices and soil properties

2.8. Validation and Accuracy of the Models

To monitor wheat growth using different datasets, including soil properties and vegetation indices, data were used individually and synergistically with applying machine learning. The predictive model accuracy performances of GPR, ER, DT, and SVM were evaluated using the RMSE, mean absolute error (MAE), and R^2 presented in the equations below, Equations (7) to (9). Both RMSE and MAE are non-negative metrics with lower values indicating better model performance. R^2 ranges from 0 to 1, where 0 indicates the model and explains none of the variance in the dependent variable, and 1 signifies a perfect fit, explaining all the variance.

$$\text{RMSE} = \sqrt{\frac{1}{n}\sum_{i=1}^{n}(P_i - O_i)^2} \tag{7}$$

$$\text{MAE} = \frac{1}{(n)}\sum_{i=1}^{n}|(P_i - O_i)| \tag{8}$$

$$R^2 = \frac{\sum_{i=1}^{n}\left(P_i - \overline{O}_i\right)^2}{\sum_{i=0}^{n}\left(P_i - \overline{O}_i\right)^2} \tag{9}$$

where n in the equations represents the number of sample points; P_i and O_i represent the estimated and observed crop height. The i and σ represent the standard deviations [102]. The crop heights measured in the field using a tape measure were compared to the values predicted by the UAV imagery to assess the validity of the models.

This study used a k-fold strategy, where k is the number of folds with a value of 10, which repeats the data split 10 times during the process for both the training and validation of models to avoid overfitting. All samples are split into 80% and 20% for both training and testing, respectively. At least for each time, random split sub-datasets were used iteratively for training and the remaining sub-subset was used for validation. Repeating the training procedure multiple times resulted in all observations for both training and validation with each observation being used for validation once [103]. This study performed assumptions' diagnosis to assess residual normality distribution in Figure A1 (Appendix A). A random distribution of the residuals was observed, which indicates that the linear model was suitable to fit wheat growth with vegetation indices and soil data measurements. The histograms showed a positive skew to the right of residuals and more residuals were closer to the straight line. In contrast, the QQ plot revealed variations in terms of distribution around the diagonal line.

3. Results

3.1. Descriptive Statistical Analysis for Soil Physical and Chemical Properties

The descriptive statistics for collected soil physical and chemical properties' measurements are presented in Table 6 for both winter wheat farms. The pH values ranged from 3.94 to 6.94, which is classified under acidic soils for both farms. However, sand was the predominant soil physical property ranging from 62 to 92%, followed by smaller amounts of clay (8–22%) and silt (0–18%). These physical properties are characteristics of loamy soils suitable for wheat growth [104]. Other soil chemical properties such as Ca, K, P, Na, and Mg show high intra-field variation in both farms, individually.

Table 6. Statistical description of soil parameters across Farm A and Farm B.

Soil Parameters	Minimum	Maximum	Mean	SD	Median	Skewness	Kurtosis
Farm A							
Clay %	8	22	13.2	2.8	12	0.8	0.6
Sand %	62	90	83.5	4.29	84	−1.8	5.9
Silt %	0	18	3.3	2.4	4	2.6	15.1
pH	3.98	6.94	5.1	0.6	5.0	0.6	0.16
Ca mg/kg	123	1570	418.6	21.5	385	2.3	9.6
K mg/kg	46	344	110.5	40.0	103.5	2.4	11.9
P mg/kg	15.3	132.9	67.1	20.3	69.6	−0.2	0.6
Na mg/kg	3.5	141	10.0	16.7	5.3	5.9	41.6
Mg mg/kg	31	338	78.2	41.7	72.5	2.9	15.4
Farm B							
Clay %	10	22	14.7	2.5	14	0.3	−0.3
Sand %	72	90	82.1	3.5	82	−0.2	−0.4
Silt %	0	6	3.2	1.5	4	−0.07	−0.3
pH	3.94	6.26	4.9	0.6	4.8	0.4	−0.3
Ca mg/kg	80	3289	442.1	382.8	382	5.7	41.9
K mg/kg	81	251	134.3	32.2	130	0.8	1.1
P mg/kg	31.2	4459.2	59.9	14.3	58.9	0.6	0.7
Na mg/kg	3.5	233	16.9	32.4	7.4	5.1	29.7
Mg mg/kg	28	202	91.5	32	85	0.7	0.71

Note: The top nine variables of Clay%; Sand%; Silt%; pH; Ca mg/kg; K mg/kg; P mg/kg; Na mg/kg; Mg mg/kg are derived from Farm A. The bottom nine variables of Clay%; Sand%; Silt%; pH; Ca mg/kg; K mg/kg; P mg/kg; Na mg/kg; Mg mg/kg are derived from Farm B.

3.2. Ordinary Kriging Semi-Variogram and Residuals for Soil Physical and Chemical Properties

This study computed the ordinary kriging spatial interpolation and evaluated the spherical, Gaussian, stable, and exponential models for experimental semi-variograms based on cross-validation. The lowest RMSE was the criteria to select optimal models in Table 7. The summary of semi-variogram model parameters included the Nugget, range (m), sill, number of lags (nlag), lag size, and Nugget/Sill ratio. The Nugget/Sill ratio (spatial dependencies) was 0–5.35 in Farm A and 0.001–6.43 in Farm B, which shows a high spatial correlation of soil physical and chemical properties in both farms [104], and the range (effective spatial dependence distance) was 100.31–575.68 and 0.001–0.009 m, which means beyond this distance there is little or no autocorrelation in the soil physical and chemical properties.

Table 7. OK best-fitted semi-variogram and residuals of model parameters for soil physical and chemical properties.

Soil Parameters	Nugget	Range (m)	Sill	Nlag	Lag Size	Nugget/Sill	RMSE	Model
Farm A								
Clay	1.93	301.09	8.22	12	33.52	0.24	1.59	Gaussian
Sand	4.85	304.29	20.85	12	33.98	0.23	2.72	Gaussian
pH	0.91	100.31	0.17	12	13.35	5.35	0.46	Gaussian
Ca	4872.53	419.81	50,983.53	12	47.55	0.09	121.45	Gaussian
K	990.94	575.68	1080.17	12	69.75	0.92	33.89	Exponential
P	0	136.33	309.69	12	16.00	0	13.83	Stable
Na	99.56	99.57	52.83	12	13.35	1.88	14.38	Spherical
Mg	579.29	308.31	1541.26	12	51.19	0.38	28.68	Stable
Farm B								
Clay	5.51	0.006	7.64	12	0.005	0.72	2.82	Circular
Sand	62.46	0.005	94.97	12	0.0004	0.66	10.74	Stable
pH	0.44	0.001	0.12	12	0.0001	3.67	0.80	Stable
Ca	185.29	0.009	185,288.60	12	0.0001	0.001	440.98	Stable
K	861.18	0.005	1138.30	12	0.0005	0.76	33.61	Stable
P	214.64	0.002	33.38	12	0.0002	6.43	15.36	Stable

Table 7. *Cont.*

Soil Parameters	Nugget	Range (m)	Sill	Nlag	Lag Size	Nugget/Sill	RMSE	Model
Na	744.86	0.006	811.83	12	0.0005	0.91	33.20	Stable
Mg	271.50	0.001	946.09	12	0.0001	0.28	29.22	Spherical

Note: The top nine variables of Clay; Sand; Silt; pH; Ca; K; P; Na; Mg are derived from Farm A. The bottom nine variables Clay; Sand; Silt; pH; Ca; K; P; Na; Mg are derived from Farm B.

The soil physical and chemical properties' spatial interpolation maps generated by ordinary kriging are presented in Figures A2 and A3 (Appendix A). These interpolation maps show a high intra-field variation of all measured soil physical and chemical properties in both winter wheat farms.

3.3. Correlation Matrix

The Pearson correlation matrix shows that soil properties—particularly Ca, Mg, K, and clay–have a moderate positive correlation with crop height compared to the vegetation indices in both winter wheat farms appearing in Figures A4 and A5, respectively. However, there was a high variability for all collected soil properties in Farm A and Farm B. For instance, Farm B had a higher correlation with actual crop height with Mg (r = 0.7), K (r = 0.61), and clay (r = 0.49) than Farm A with Mg (r = 0.34), k (r = 0.33), and clay (r = 0.18). The difference in both soil chemical and physical properties' correlation can be attributed to an imbalance in the fertilisation rate and the availability of nutrients.

3.4. Model Validation

The performance of the GPR, ER, DT, and SVM models' accuracy statistics is summarised in Table 8 (Farm A) and Table 9 (Farm B). The GPR (R^2 = 0.69 to 0.74, RMSE = 15.95 to 17.91 cm) model performed better than ER (R^2 = 0.67 to 0.70 and RMSE = 17.13 to 18.68 cm) and other models for both farms using vegetation indices as input features, respectively. The UAV-derived vegetation indices' input features showed a slight improvement in model accuracies compared to the data fusion of vegetation indices and soil properties scenario. Overall, the evaluated GPR, ER, DT, and SVM models achieved a satisfactory accuracy result with training datasets. However, the minimal difference between the training and testing sets shows that sufficient data were used to reduce model overfitting. The difference between the training and testing datasets was minimal with an R^2 of 0.62–0.78 for Farm A and an R^2 of 0.5–0.69 for Farm B. This validates the model and indicates the robustness of the model in handling variations.

Table 8. GPR, ER, DT, and SVM model evaluation statistics for Farm A.

Wheat Farm	Predictor Variables	Model	Training Set			Testing Set		
			R^2	RMSE	MAE	R^2	RMSE	MAE
Farm A	Vegetation indices	GPR	0.74	15.95	11.59	0.73	16.67	11.64
	Vegetation indices	ER	0.70	17.13	12.58	0.69	18.14	12.97
	Vegetation indices	DT	0.69	17.36	12.46	0.62	19.90	13.26
	Vegetation indices	SVM	0.64	18.58	14.23	0.63	19.58	14.00
	Vegetation indices and soil properties	GPR	0.73	16.41	11.69	0.78	14.47	11.07
	Vegetation indices and soil properties	ER	0.68	17.84	12.87	0.77	17.93	10.98
	Vegetation indices and soil properties	DT	0.67	18.04	13.18	0.73	15.97	12.29
	Vegetation indices and soil properties	SVM	0.62	19.37	14.99	0.71	16.63	13.23

Table 9. GPR, ER, DT, and SVM model evaluation statistics for Farm B.

Wheat Farm	Predictor Variables	Model	Training Set			Testing Set		
			R^2	RMSE	MAE	R^2	RMSE	MAE
Farm B	Vegetation indices	GPR	0.69	17.91	11.87	0.61	19.71	13.36
	Vegetation indices	ER	0.67	18.68	12.05	0.58	20.29	14.17
	Vegetation indices	DT	0.67	18.69	11.92	0.58	20.26	13.87
	Vegetation indices	SVM	0.67	18.55	13.68	0.58	20.43	15.74
	Vegetation indices and soil properties	GPR	0.65	19.07	13.09	0.68	18.14	12.65
	Vegetation indices and soil properties	ER	0.63	16.61	13.66	0.66	18.62	13.29
	Vegetation indices and soil properties	DT	0.61	20.17	13.05	0.66	18.60	11.93
	Vegetation indices and soil properties	SVM	0.58	20.75	15.74	0.50	22.68	17.74

The best-performing GPR model was used to produce scatterplots using training datasets. The data points close to the diagonal line show a good agreement between measured and predicted crop height values. The GPR model produced with vegetation indices' training data had a slightly better performance (R^2 = 0.74, RMSE = 15.95, and MAE = 11.59) compared to the GPR model (R^2 = 0.73, RMSE = 16.41, and MAE = 11.69) generated using a soil properties and vegetation indices data fusion for Farm A (Figure 7). Similar results were observed in Farm B when the GPR model achieved a coefficient of determination of 0.4 with vegetation indices' input features (Figure 8).

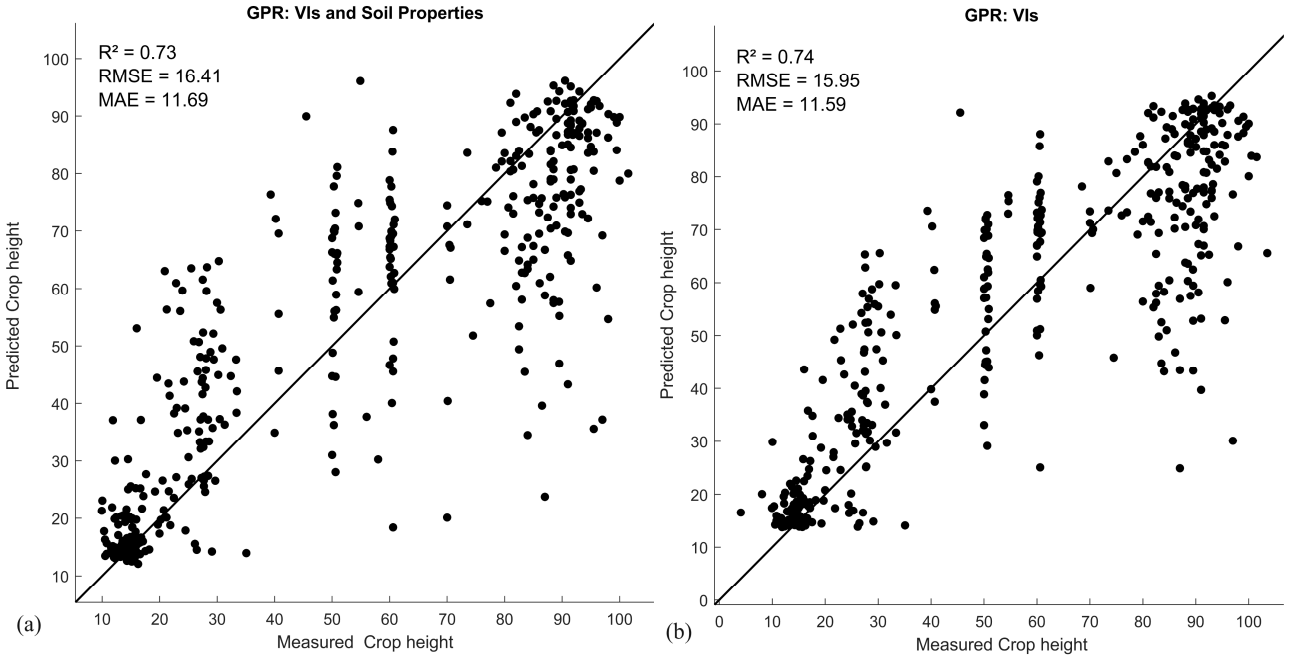

Figure 7. Farm A scatterplots showing the relationship between predicted and observed crop height using the GPR model with (**a**) vegetation indices and soil properties data fusion and (**b**) vegetation-index-only scenario.

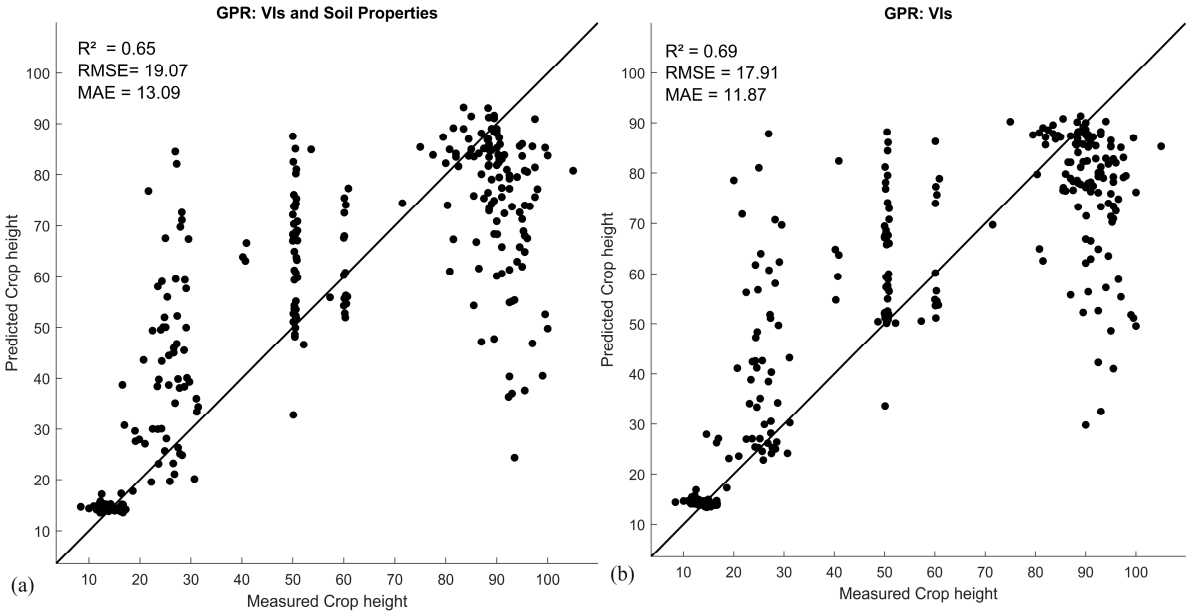

Figure 8. Farm B scatterplots showing the relationship between predicted and observed crop height using the GPR model with (**a**) vegetation indices and soil properties data fusion and (**b**) vegetation-index-only scenario.

3.5. GPR Model Variable Importance

The GPR robust performance model was used to rank the importance of predictor variables using the training data for different farms, respectively (Figure 9). The most important input features for GPR were RENDVI and NDI in Farm A, while RENDVI, RVI2, and NDVI ranked highly for the GPR model in Farm B. pH is the only soil chemical property that had a lower ranking in Farm A, while other soil properties had no contribution in both farm experiments.

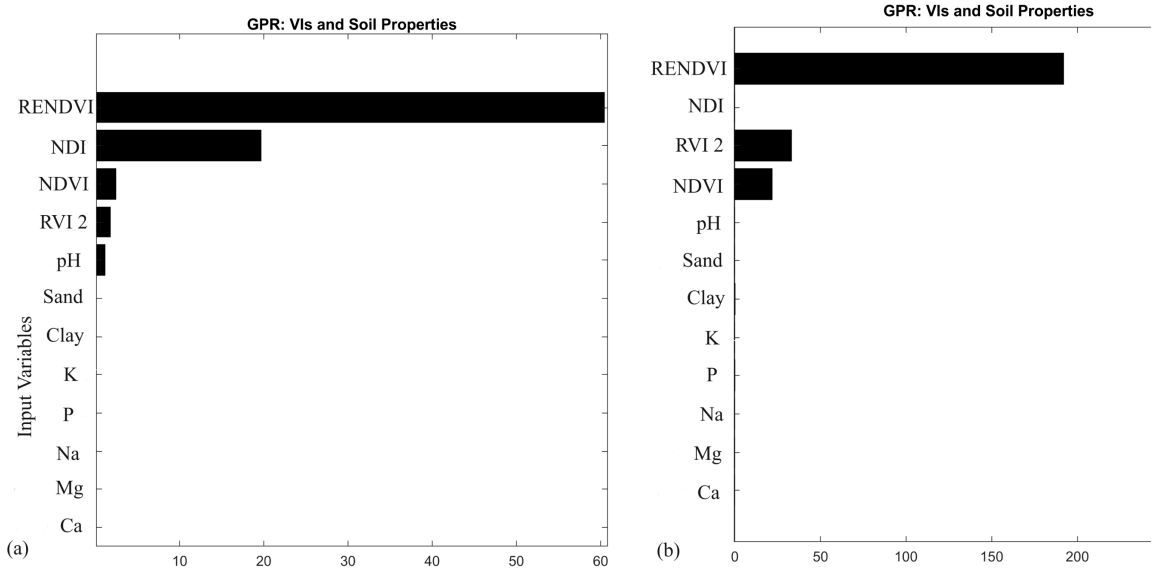

Figure 9. Variable importance feature performance of vegetation indices and soil properties within (**a**) Farm A and (**b**) Farm B in the GPR algorithm.

4. Discussion

According to descriptive statistics, the soil pH of both farms is acidic, ranging from 3.5 to 6.94. The range of the pH conforms with previous findings that indicate a pH of about

5.5 in the study area [105]. This scenario is anticipated in dryland wheat production within the study area. Low pH is detrimental to wheat growth [106,107]. Furthermore, results revealed that soil properties, particularly Ca, Mg, K, and clay, have a moderate positive correlation with wheat crop height. Similar findings from other studies have revealed that an abundance of soil chemical properties such as K, Mg, and Ca have an influence on the wheat crop height throughout the growth period [7,21,59]. Other studies also demonstrated that the clay content, silt%, and pH values are more significant factors influencing plant growth [8,104]. Vegetation indices showed a weak positive correlation with wheat crop height. In contrast, other studies found a strong correlation between vegetation indices and wheat height and yields [108,109]. Additionally, the correlation increases as the winter wheat grows [108]. Ordinary kriging is widely known for its ability to generate spatial interpolation maps in precision agriculture applications [110–112]. This study confirmed that ordinary kriging is a robust method to produce soil property maps for both farms based on the low cross-validation RSME of semi-variogram models.

Four predictive machine learning models were evaluated. Results show that the GPR model outperformed ER, DT, and SVM models when predicting crop height at the wheat farms. The GPR model prediction accuracy results ranged between 65% and 75% for wheat height in the entire season. These results are better than findings from previous studies that obtained a 13% to 84% prediction accuracy for monitoring winter wheat growth using the PLSR model during the entire growing season [113]. Other studies have found 68%, 88%, and 90% prediction accuracy of field-scale wheat biophysical variables, wheat yield, and wheat plant nitrogen density using the GPR model [44,45,114]. These findings are similar to previous studies that showed the higher capabilities of GPR modelling performance compared to algorithms such as LR, RF, PLSR, LSLR, BagT, KNN, DT, NNs, ANN, and RegT when estimating different crop biophysical parameters [34,44,46,114]. Furthermore, the result showed that the GPR model has a lower prediction accuracy with soil and UAV imagery derived from data fusion compared with the UAV vegetation indices scenario. In contrast, previous research showed that hyperspectral UAV and soil data fusion improve GPR modelling precision while providing more accurate results with vegetation indices for estimating wheat above-ground biomass [42,115]. The improved performance of GPR can be linked to its use of kernel functions when dealing with input [46,47,82]. Furthermore, GPR is flexible and reduces the potential of overfitting with highly dimensional observations in crop parameter estimation [42,50,116,117]. In contrast, other studies show that PLSR and SVM achieved the highest prediction modelling accuracy compared to GPR for wheat crop height, above-ground biomass, and wheat yield [35,44]. Additionally, ANN and RF have outperformed the GPR model for plant height and biomass estimation in previous studies [118,119]. However, the robustness of the MLA model depends on the amount of input data and its features to calibrate nonlinear and complex data structures [42,45,46]. Despite the advantages of the GPR model such as the kernel function when dealing with the input training data, it cannot be generalised that GPR always performs better than other machine learning models.

The GPR model variable importance analysis indicates that RENDVI is vital for predicting wheat crop height. A similar study revealed that vegetation indices such as the enhanced vegetation index (EVI) performed better than soil properties in modelling crop height [44,113]. These findings showed that the vegetation indices, especially those using the red-edge band, are superior for forecasting crop growth. Several studies have concluded that red-edge bands are anticipated to have a higher-ranking variable of importance in predicting crop growth because of their higher sensitivity in crop changes [31,120]. Moreover, the wheat crop height changes throughout the season could have influenced the top ranking of RENDVI computed with red-edge bands in the current study. Meanwhile, this study showed that soil properties play a lesser role when estimating wheat crop height. pH had a lower ranking in all soil properties used to estimate crop growth. All other soil properties such as sand, clay, Na, Mg, Ca, K, and P showed no contribution to the GPR variable importance. However, previous studies highlighted contrasting findings that pH

and K are top-ranking soil properties [7,14]. In addition, random forest variable importance has revealed that the Ca_Mg ratio ranked highly compared to other soil properties and vegetation indices in soil organic carbon content [121]. It is worth noting that clay plays a very important role in growing crops, whereas sand is not an ideal environment for growing crops [104]. The changes within findings of variable importance are attributed to differences in the model input predictor variables. Understanding the different growth stages helps farmers plan and implement appropriate agricultural practices, such as timing irrigation, fertilization, and harvesting. The techniques developed in this study can be used in other semi-arid regions facing challenges related to optimising crop yield, resource management, and sustainable agriculture practices [52].

This study highlights the importance of vegetation indices and soil properties to predict crop height, which provides valuable information about basic crop management. However, the limitation of this research includes high fieldwork costs that resulted in one visit per month for data collection at different crop development stages. This study focused on time-series modelling but may not fully capture the temporal dynamics of wheat growth. The effects of short-term environmental fluctuations and seasonal variations on crop growth may not be adequately addressed. This study acknowledges that vegetation indices' reflectance can be affected by various factors such as surface temperature, atmospheric distortions, ambient light, water content, and vegetation type. These factors could introduce uncertainties in the accuracy of the models. We recommend incorporating climate data, soil indices, and environmental variables for a holistic understanding of crop growth while optimising model estimation accuracy. Furthermore, we recommend to investigate the benefits of fusing data from multiple sensors, such as thermal imaging, LiDAR, and hyperspectral sensors. This can provide a more comprehensive characterisation of crop health and growth status.

5. Conclusions

This study evaluates UAV-derived vegetation indices and soil properties to predict winter wheat growth at two identical farms. Vegetation indices and soil properties' predictor variables were related to crop height. The red-edge and NIR bands were highly sensitive to the surface reflectance of wheat growth. Clay, Ca, Mg, and K soil properties were related to wheat crop height with a positive correlation between 0.18 and 0.7. All the evaluated machine learning models including GPR, ER, DT, and SVM produced reasonable accuracies for crop height prediction. Additionally, model performance findings show that GPR (R^2 = 0.69 to 0.74, RMSE = 15.95 to 17.91 cm) has a high predictive capacity for crop height in both wheat farms. Variable importance highlighted RENDVI as the most influential predictor variable in the GPR model. The methodology developed in this study can help farmers improve farm management practices such as timing irrigation, fertilization, and harvesting. Extension services can also benefit from recommending site-specific crop management decisions to increase expected yields while improving food security. The research prospects may include seasonal datasets to understand variations and identify appropriate windows for early production assessment. Additionally, they can examine wheat physiological stresses and yield data to predict crop productivity.

Author Contributions: Conceptualization, L.N. and C.M.; methodology, L.N. and C.M.; software and data pre-processing, L.N. and C.M.; writing—original draft preparation, L.N.; writing—review and editing, C.M., J.G.C., A.M.K., Z.M.-M., W.M. and P.E.R.; supervision, J.G.C., C.M., A.M.K., Z.M.-M. and W.M. All authors have read and agreed to the published version of the manuscript.

Funding: This research was funded by the Council for Scientific and Industrial Research (CSIR) and the Department of Science and Innovation (DSI). Research support from the Agricultural Research Council-Natural Resources and Engineering (ARC-NRE), National Research Foundation (NRF) (grant number: TTK200221506319), and the South African National Space Agency (SANSA) is acknowledged.

Data Availability Statement: The raw data supporting the conclusions of this article will be made available by the authors on request.

Acknowledgments: The authors would like to thank the Agricultural Research Council (ARC-NRE) and the University of Pretoria for creating an enabling environment for research. We would also like to thank the following people for participating in the field campaigns: Cilence Munghemezulu, Eric Economon, Pisto Khoboko, Phathutshedzo Eugene Ratshiedana, and Wonga Masiza.

Conflicts of Interest: The authors declare no conflicts of interest.

Appendix A

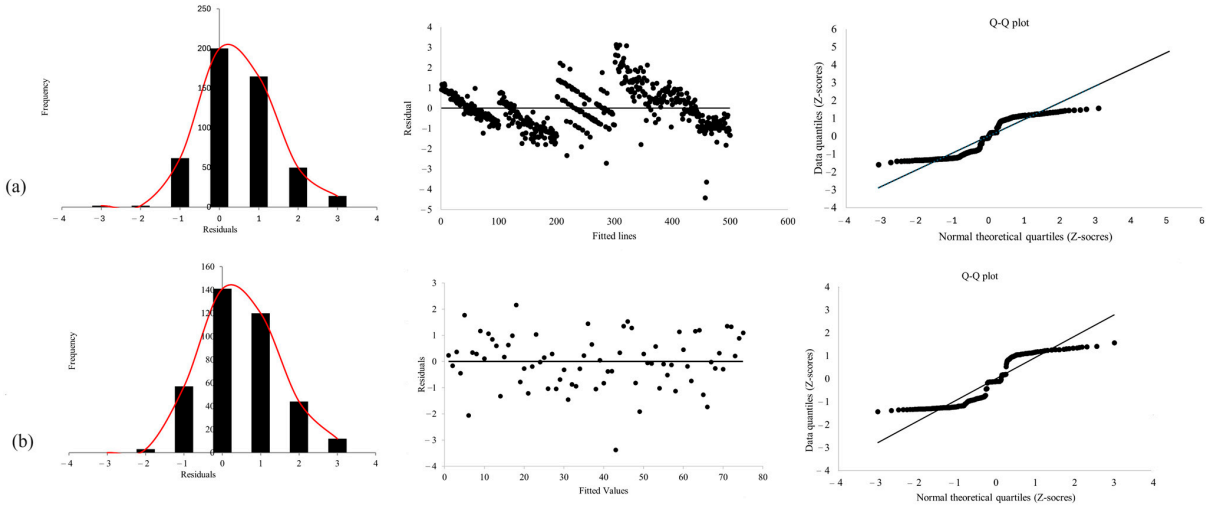

Figure A1. Model assumption plots for residual normality distributed using histogram, linear model and QQ plot normality plot fitted appropriately from the data; (**a**) Farm A and (**b**) Farm B. Red line show distribution of the data.

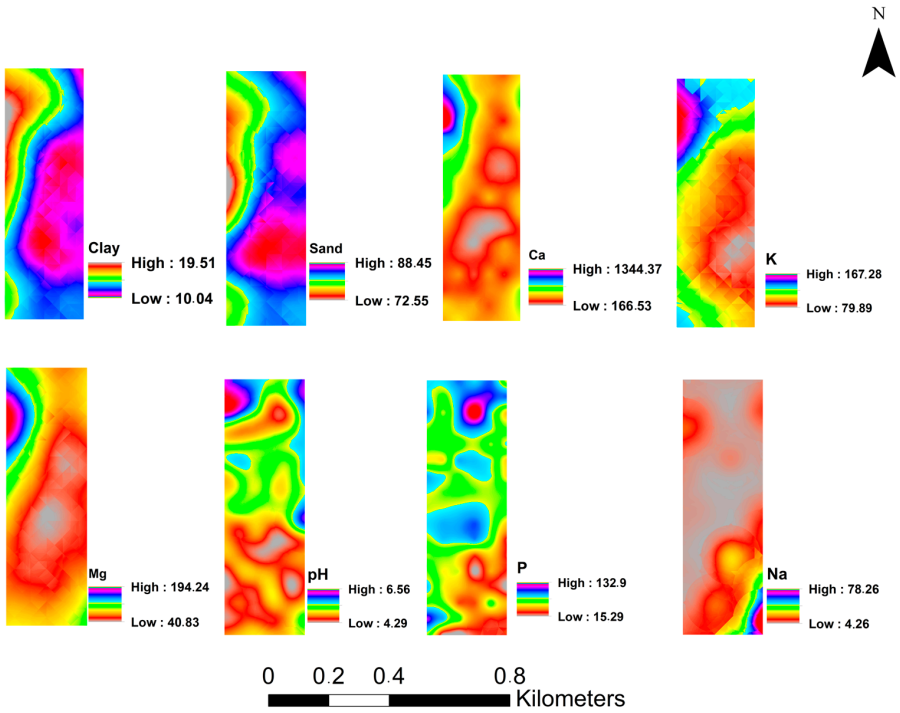

Figure A2. Farm A ordinary kriging spatial interpolation maps of soil physical and chemical properties of sampled points.

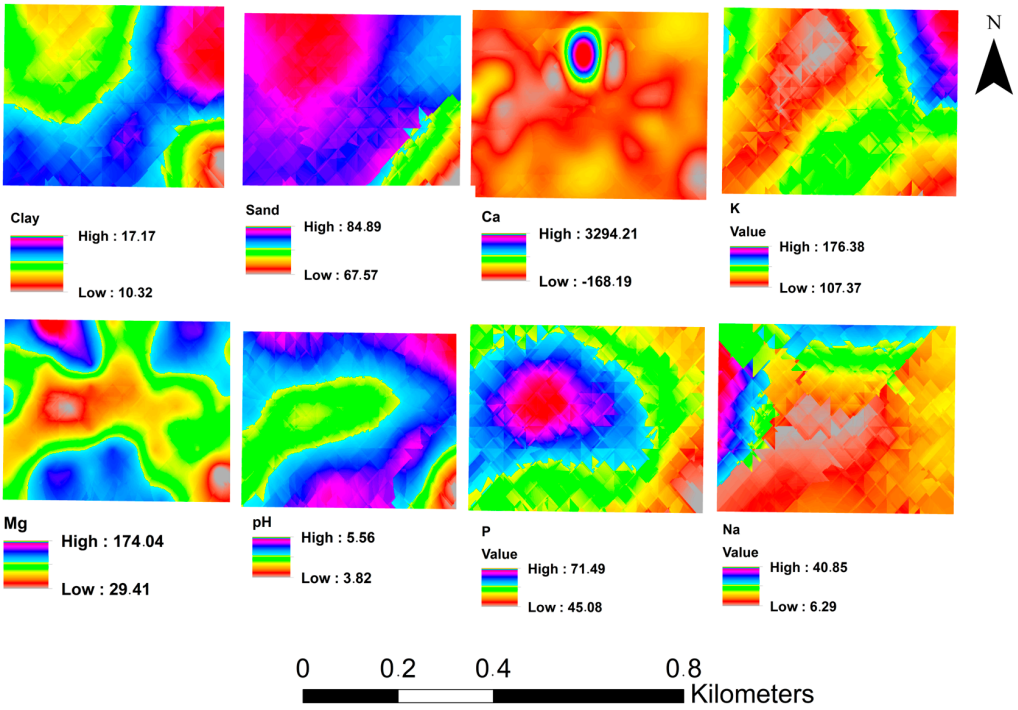

Figure A3. Farm B ordinary kriging spatial interpolation maps of soil physical and chemical properties of sampled points.

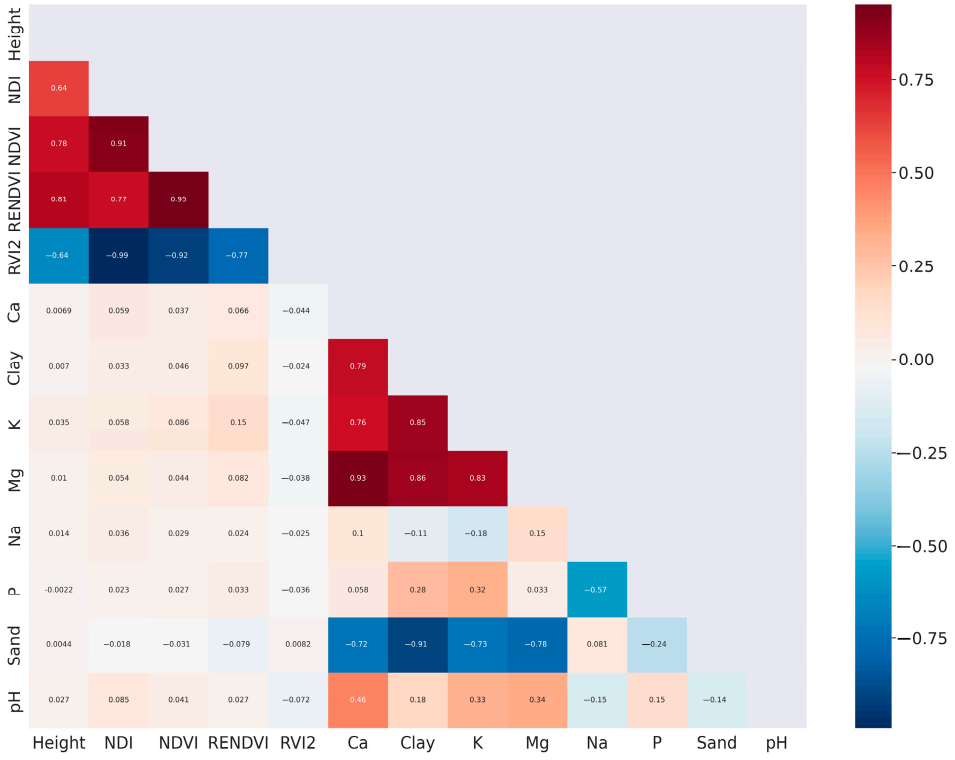

Figure A4. Farm A: Pearson correlation matrix of vegetation indices and soil physical and chemical properties.

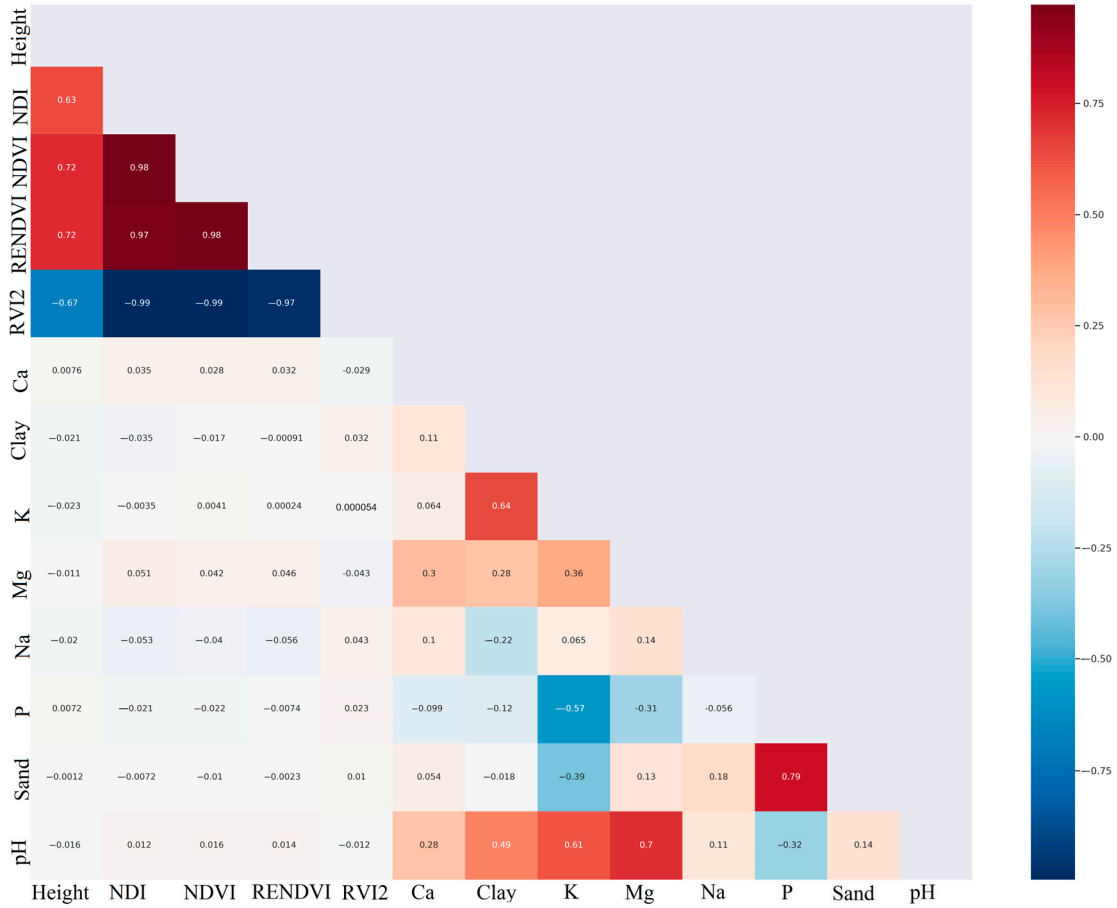

Figure A5. Farm B: Pearson correlation matrix of vegetation indices and soil physical and chemical properties.

References

1. Florence, A.; Revill, A.; Hoad, S.; Rees, R.; Williams, M. The Effect of Antecedence on Empirical Model Forecasts of Crop Yield from Observations of Canopy Properties. *Agriculture* **2021**, *11*, 258. [CrossRef]
2. Erenstein, O.; Jaleta, M.; Mottaleb, K.A.; Sonder, K.; Donovan, J.; Braun, H.J. Global Trends in Wheat Production, Consumption and Trade. In *Wheat Improvement*; Reynolds, M.P., Braun, H.-J., Eds.; Springer International Publishing: Cham, Switzerland, 2022; pp. 47–66. [CrossRef]
3. Nduku, L.; Munghemezulu, C.; Mashaba-Munghemezulu, Z.; Kalumba, A.M.; Chirima, G.J.; Masiza, W.; De Villiers, C. Global Research Trends for Unmanned Aerial Vehicle Remote Sensing Application in Wheat Crop Monitoring. *Geomatics* **2023**, *3*, 115–136. [CrossRef]
4. ELSabagh, A.; Islam, M.S.; Skalicky, M.; Ali Raza, M.; Singh, K.; Anwar Hossain, M.; Arshad, A. Salinity Stress in Wheat (*Triticum aestivum* L.) in the Changing Climate: Adaptation and Management Strategies. *Front. Agron.* **2021**, *3*, 661932. [CrossRef]
5. Nduku, L.; Munghemezulu, C.; Mashaba-Munghemezulu, Z.; Kalumba, A.; Masiza, W.; Ratshiedana, P.; Chirima, G. Modelling of Intra-field Winter Wheat Crop Growth Variability Using In Situ Measurements, UAV derived Vegetation Indices, Soil Properties, and Machine Learning Algorithms. In Proceedings of the 5th International Electronic Conference on Remote Sensing, Online, 7–21 November 2023; MDPI: Basel, Switzerland, 2023. [CrossRef]
6. Alexandratos, N.; Bruinsma, J. *World Agriculture towards 2030/2050: The 2012 Revision*; ESA Working Papers 12-03; FAO: Rome, Italy, 2012.
7. Goffart, D.; Dvorakova, K.; Crucil, G.; Curnel, Y.; Limbourg, Q.; Van Oost, K.; Van Wesemael, B. UAV Remote Sensing for Detecting Within-Field Spatial Variation of Winter Wheat Growth and Links to Soil Properties and Historical Management Practices. A Case Study on Belgian Loamy Soil. *Remote Sens.* **2022**, *14*, 2806. [CrossRef]
8. Giraldo, P.; Benavente, E.; Manzano-Agugliaro, F.; Gimenez, E. Worldwide Research Trends on Wheat and Barley: A Bibliometric Comparative Analysis. *Agronomy* **2019**, *9*, 352. [CrossRef]
9. Qi, H.; Paz-Kagan, T.; Karnieli, A.; Li, S. Linear Multi-Task Learning for Predicting Soil Properties Using Field Spectroscopy. *Remote Sens.* **2017**, *9*, 1099. [CrossRef]
10. Yang, T.; Siddique, K.H.; Liu, K. Cropping Systems in Agriculture and Their Impact on Soil Health—A Review. *Glob. Ecol. Conserv.* **2020**, *23*, e01118. [CrossRef]

11. Borole, V.Y.; Kulkarni, S.B. Soil Properties Classification Using Support Vector Machine for Raver Tehsil. *Int. J. Adv. Trends Comput. Sci. Eng.* **2021**, *10*, 3154–3159. [CrossRef]
12. Rossel, R.V.; Behrens, T.; Ben-Dor, E.; Brown, D.J.; Demattê, J.A.M.; Shepherd, K.D.; Ji, W. A Global Spectral Library to Characterize the World's Soil. *Earth-Sci. Rev.* **2016**, *155*, 198–230. [CrossRef]
13. Webb, H.; Barnes, N.; Powell, S.; Jones, C. Does Drone Remote Sensing Accurately Estimate Soil pH in a Spring Wheat Field in Southwest Montana? *Precis. Agric.* **2021**, *22*, 1803–1815. [CrossRef]
14. Johnston, A.E. Soil Acidity—Resilience and Thresholds. In *Managing Soil Quality: Challenges in Modern Agriculture*, 1st ed.; Schjønning, P., Elmholt, S., Christensen, B.T., Eds.; CABI Publishing: Wallingford, UK, 2004; pp. 35–46. [CrossRef]
15. Hocking, P.J. Dry-matter Production, Mineral Nutrient Concentrations, and Nutrient Distribution and Redistribution in Irrigated Spring Wheat. *J. Plant Nutr.* **1994**, *17*, 1289–1308. [CrossRef]
16. Wenjun, J.; Zhou, S.; Jingyi, H.; Shuo, L. In Situ Measurement of Some Soil Properties in Paddy Soil Using Visible and Near-Infrared Spectroscopy. *PLoS ONE* **2014**, *9*, e105708. [CrossRef]
17. Trontelj ml, J.; Chambers, O. Machine Learning Strategy for Soil Nutrients Prediction Using Spectroscopic Method. *Sensors* **2021**, *21*, 4208. [CrossRef]
18. Zhu, Y.; Liu, J.; Tao, X.; Su, X.; Li, W.; Zha, H.; Li, X. A Three-Dimensional Conceptual Model for Estimating the Above-Ground Biomass of Winter Wheat Using Digital and Multispectral Unmanned Aerial Vehicle Images at Various Growth Stages. *Remote Sens.* **2023**, *15*, 3332. [CrossRef]
19. Ayala-Silva, T.; Beyl, C.A. Changes in Spectral Reflectance of Wheat Leaves in Response to Specific Macronutrient Deficiency. *Adv. Space Res.* **2005**, *35*, 305–317. [CrossRef]
20. Kajla, M.; Yadav, V.K.; Khokhar, J.; Singh, S.; Chhokar, R.S.; Meena, R.P.; Sharma, R.K. Increase in Wheat Production through Management of Abiotic Stresses: A Review. *J. Appl. Nat. Sci.* **2015**, *7*, 1070–1080. [CrossRef]
21. Skendžić, S.; Zovko, M.; Lešić, V.; Pajač Živković, I.; Lemić, D. Detection and Evaluation of Environmental Stress in Winter Wheat Using Remote and Proximal Sensing Methods and Vegetation Indices—A Review. *Diversity* **2023**, *15*, 481. [CrossRef]
22. Balachandran, S.; Hurry, V.M.; Kelley, S.E.; Osmond, C.B.; Robinson, S.A.; Rohozinski, J.; Sims, D.A. Concepts of Plant Biotic Stress. Some Insights into the Stress Physiology of Virus-Infected Plants, from the Perspective of Photosynthesis. *Physiol. Plant.* **1997**, *100*, 203–213. [CrossRef]
23. Higley, L.G.; Browde, J.A.; Higley, P.M. Moving Towards New Understandings of Biotic Stress and Stress Interactions. In *Humic Substances and Chemical Contaminants*; Wiley: Hoboken, NJ, USA, 2015; pp. 749–754.
24. Shew, A.M.; Tack, J.B.; Nalley, L.L.; Chaminuka, P. Yield Reduction under Climate Warming Varies among Wheat Cultivars in South Africa. *Nat. Commun.* **2020**, *11*, 4408. [CrossRef]
25. Skendžić, S.; Zovko, M.; Lešić, V.; Pajač Živković, I.; Lemić, D. The Impact of Climate Change on Agricultural Insect Pests. *Insects* **2021**, *12*, 440. [CrossRef] [PubMed]
26. Tucker, C.J. Red and Photographic Infrared Linear Combinations for Monitoring Vegetation. *Remote Sens. Environ.* **1979**, *8*, 127–150. [CrossRef]
27. Bannari, A.; Morin, D.; Bonn, F.; Huete, A. A Review of Vegetation Indices. *Remote Sens. Rev.* **1995**, *13*, 95–120. [CrossRef]
28. Herbei, M.; Jurescu, A.L.; Florin, S.A.L.A. Evaluation of the Wheat Crop and Production Estimation Based on Remote Sensing. *Life Sci. Sustain. Dev.* **2023**, *4*, 93–100. Available online: https://www.lssd-journal.com (accessed on 10 June 2023). [CrossRef]
29. Ziliani, M.G.; Parkes, S.D.; Hoteit, I.; McCabe, M.F. Intra-Season Crop Height Variability at Commercial Farm Scales Using a Fixed-Wing UAV. *Remote Sens.* **2018**, *10*, 2007. [CrossRef]
30. Tao, H.; Feng, H.; Xu, L.; Miao, M.; Yang, G.; Yang, X.; Fan, L. Estimation of the Yield and Plant Height of Winter Wheat Using UAV-Based Hyperspectral Images. *Sensors* **2020**, *20*, 1231. [CrossRef] [PubMed]
31. Xue, J.; Su, B. Significant Remote Sensing Vegetation Indices: A Review of Developments and Applications. *J. Sens.* **2017**, *2017*, 1353691. [CrossRef]
32. Wang, D.; Li, R.; Zhu, B.; Liu, T.; Sun, C.; Guo, W. Estimation of Wheat Plant Height and Biomass by Combining UAV Imagery and Elevation Data. *Agriculture* **2022**, *13*, 9. [CrossRef]
33. Selige, T.; Böhner, J.; Schmidhalter, U. High Resolution Topsoil Mapping Using Hyperspectral Image and Field Data in Multivariate Regression Modeling Procedures. *Geoderma* **2006**, *136*, 235–244. [CrossRef]
34. Naidoo, L.; Main, R.; Cho, M.A.; Madonsela, S.; Majozi, N. Machine Learning Modelling of Crop Structure within the Maize Triangle of South Africa. *Int. J. Remote Sens.* **2022**, *43*, 27–51. [CrossRef]
35. Wang, Y.; Zhu, D.; Ding, Y. Identification of Winter Wheat-Growing Areas Based on the XGBoost Algorithm. *Preprints* **2023**, *1*, 2–13. [CrossRef]
36. Vohland, M.; Emmerling, C. Determination of Total Soil Organic C and Hot Water-Extractable C from VIS-NIR Soil Reflectance with Partial Least Squares Regression and Spectral Feature Selection Techniques. *Eur. J. Soil Sci.* **2011**, *62*, 598–606. [CrossRef]
37. Monteiro-Silva, F.; Jorge, P.A.; Martins, R.C. Optical Sensing of Nitrogen, Phosphorus and Potassium: A Spectrophotometrical Approach Toward Smart Nutrient Deployment. *Chemosensors* **2019**, *7*, 51. [CrossRef]
38. Angelopoulou, T.; Balafoutis, A.; Zalidis, G.; Bochtis, D. From Laboratory to Proximal Sensing Spectroscopy for Soil Organic Carbon Estimation—A Review. *Sustainability* **2020**, *12*, 443. [CrossRef]
39. Oshiro, T.M.; Perez, P.S.; Baranauskas, J.A. How many trees in a random forest. In *International Workshop on Machine Learning and Data Mining in Pattern Recognition*; Springer: Berlin/Heidelberg, Germany, 2012; pp. 154–168.

40. Probst, P.; Boulesteix, A.-L. To tune or not to tune the number of trees in random forest. *J. Mach. Learn. Res.* **2017**, *18*, 6673–6690.
41. Żelazny, W.R.; Kusnierek, K.; Geipel, J. Gaussian Process Modeling of In-Season Physiological Parameters of Spring Wheat Based on Airborne Imagery from Two Hyperspectral Cameras and Apparent Soil Electrical Conductivity. *Remote Sens.* **2022**, *14*, 5977. [CrossRef]
42. Verrelst, J.; Malenovský, Z.; Van der Tol, C.; Camps-Valls, G.; Gastellu-Etchegorry, J.P.; Lewis, P.; North, P.; Moreno, J. Quantifying Vegetation Biophysical Variables from Imaging Spectroscopy Data: A Review on Retrieval Methods. *Surv. Geophys.* **2019**, *40*, 589–629. [CrossRef] [PubMed]
43. Han, J.; Zhang, Z.; Cao, J.; Luo, Y.; Zhang, L.; Li, Z.; Zhang, J. Prediction of Winter Wheat Yield Based on Multi-Source Data and Machine Learning in China. *Remote Sens.* **2020**, *12*, 236. [CrossRef]
44. Fu, Y.; Yang, G.; Li, Z.; Song, X.; Li, Z.; Xu, X.; Zhao, C. Winter Wheat Nitrogen Status Estimation Using UAV-Based RGB Imagery and Gaussian Processes Regression. *Remote Sens.* **2020**, *12*, 3778. [CrossRef]
45. Upreti, D.; Huang, W.; Kong, W.; Pascucci, S.; Pignatti, S.; Zhou, X.; Casa, R. A Comparison of Hybrid Machine Learning Algorithms for the Retrieval of Wheat Biophysical Variables from Sentinel-2. *Remote Sens.* **2019**, *11*, 481. [CrossRef]
46. Camps-Valls, G.; Bruzzone, L. *Kernel Methods for Remote Sensing Data Analysis*, 1st ed.; Wiley: Hoboken, NJ, USA, 2009. [CrossRef]
47. Verrelst, J.; Alonso, L.; Caicedo, J.P.R.; Moreno, J.; Camps-Valls, G. Gaussian Process Retrieval of Chlorophyll Content from Imaging Spectroscopy Data. *IEEE J. Sel. Top. Appl. Earth Obs. Remote Sens.* **2013**, *6*, 867–874. [CrossRef]
48. Pasolli, E.; Melgani, F.; Alajlan, N.; Bazi, Y. Active Learning Methods for Biophysical Parameter Estimation. *IEEE Trans. Geosci. Remote Sens.* **2012**, *50*, 4071–4084. [CrossRef]
49. Verrelst, J.; Rivera, J.P.; Gitelson, A.; Delegido, J.; Moreno, J.; Camps-Valls, G. Spectral Band Selection for Vegetation Properties Retrieval Using Gaussian Processes Regression. *Int. J. Appl. Earth Obs. Geoinf.* **2016**, *52*, 554–567. [CrossRef]
50. Li, M.; Shamshiri, R.R.; Weltzien, C.; Schirrmann, M. Crop Monitoring Using Sentinel-2 and UAV Multispectral Imagery: A Comparison Case Study in Northeastern Germany. *Remote Sens.* **2022**, *14*, 4426. [CrossRef]
51. Lamprecht, R. Dihlabeng Local Municipality Sewer Bridge and Pipeline Development, Paul Roux, Free State Province. Available online: https://sahris.sahra.org.za/sites/default/files/additionaldocs/PR%20Sewer%20Pipe%20Bridge%20FBAR.pdf (accessed on 30 June 2023).
52. Wang, B.; Liu, D.L.; O'Leary, G.J.; Asseng, S.; Macadam, I.; Lines-Kelly, R.; Yang, X.; Clark, A.; Crean, J.; Sides, T.; et al. Australian Wheat Production Expected to Decrease by the Late 21st Century. *Glob. Chang. Biol.* **2018**, *24*, 2403–2415. [CrossRef]
53. Joshi, K.D.; Rehman, A.U.; Ullah, G.; Nazir, M.F.; Zahara, M.; Akhtar, J.; Imtiaz, M. Acceptance and Competitiveness of New Improved Wheat Varieties by Smallholder Farmers. *J. Crop Improv.* **2017**, *31*, 608–627. [CrossRef]
54. Moffett, R. *A Field Guide to the Clarens Village Conservancy*; AFRICAN SUN MEDIA; University of the Free State: Bloemfontein, South Africa, 2018. [CrossRef]
55. Sekhele, N.M. Assessing the Effects of Grazing on Vegetation Cover and Associated Socio-Economic Livelihoods in the Clarens Nature Reserve in the Free State, South Africa. 2018. Available online: http://scholar.ufs.ac.za/xmlui/handle/11660/10141. (accessed on 29 August 2023).
56. Hensley, M.; Le Roux, P.; Du Preez, C.; Van Huyssteen, C.; Kotze, E.; Van Rensburg, L. Soils: The Free State agricultural base. *S. Afr. Geogr. J.* **2006**, *88*, 11–21. [CrossRef]
57. Mashaba, Z. Modelling Dryland Winter Wheat Yield Using Remotely Sensed Imagery and Agrometeorological Parameters. University of Pretoria. 2017. Available online: https://repository.up.ac.za/handle/2263/60634 (accessed on 16 September 2023).
58. Loke, P.F.; Schimper, J.J.; Kotzé, E.; du Preez, C.C. Long-Term Wheat Production Management Effects on Soil Fertility In-dicators in the Semi-Arid Eastern Free State, South Africa. *S. Afr. J. Plant Soil* **2021**, *38*, 93–106. [CrossRef]
59. Moeletsi, M.E.; Tongwane, M.; Tsubo, M. The Study of Frost Occurrence in Free State Province of South Africa. *Adv. Meteorol.* **2016**, *2016*, 9586150. [CrossRef]
60. Mbiriri, M.; Mukwada, G.; Manatsa, D. Influence of Altitude on the Spatiotemporal Variations of Meteorological Droughts in Mountain Regions of the Free State Province, South Africa (1960–2013). *Adv. Meteorol.* **2018**, *2018*, 5206151. [CrossRef]
61. Myeni, L.; Moeletsi, M.; Thavhana, M.; Randela, M.; Mokoena, L. Barriers Affecting Sustainable Agricultural Productivity of Smallholder Farmers in the Eastern Free State of South Africa. *Sustainability* **2019**, *11*, 3003. [CrossRef]
62. Le Roux, A.; Van Niekerk, C.W.; Arnold, K.A.; Pieterse, A.; Davis, C.L. What to Adapt for? Climate Change Risk Profiles for South African Cities. Available online: https://s3-eu-west-1.amazonaws.com/csir-greenbook/resources/LeRoux.etal_What_to_Adapt_for_2018.pdf (accessed on 15 June 2023).
63. Lamula, S.Q.N. Characterization of Wheat Nematodes from Cultivars in South Africa. North-West University (South Africa). 2020. Available online: https://repository.nwu.ac.za/handle/10394/35175 (accessed on 25 September 2023).
64. Rodrigues, G.C.; Braga, R.P. Evaluation of NASA POWER Reanalysis Products to Estimate Daily Weather Variables in a Hot Summer Mediterranean Climate. *Agronomy* **2021**, *11*, 1207. [CrossRef]
65. Michaelson, G.J.; Ping, C.L.; Mitchell, G.A. Correlation of Mehlich 3, Bray 1, and Ammonium Acetate Extractable P, K, Ca, and Mg for Alaska Agricultural Soils. *Commun. Soil Sci. Plant Anal.* **1987**, *18*, 1003–1015. [CrossRef]
66. Lakanen, E.; Ervio, R. A Comparison of Eight Extractants for the Determination of Plant Available Micronutrients in Soils. *Acta Agral. Fenn.* **1971**, *123*, 223–232.
67. Doll, E.C.; Lucas, R.E. Testing Soils for Potassium, Calcium and Magnesium. In *Soil Testing and Plant Analysis*; Walsh, L.M., Beaton, J.D., Eds.; Soil Science Society of America Inc.: Madison, WI, USA, 1973; pp. 133–151.

68. Kome, G.K.; Enang, R.K.; Yerima, B.P.K.; Lontsi, M.G.R. Models Relating Soil pH Measurements in H2O, KCl and CaCl2 for Volcanic Ash Soils of Cameroon. *Geoderma Reg.* **2018**, *14*, e00185. [CrossRef]
69. AFNOR. NF X31–107. In *Soil Quality—Particle Size Determination by Sedimentation—Pipette Method*; AFNOR: Saint-Denis La Plaine, France, 2003.
70. *Pix4D*; Pix4Dmapper 4.1 User Manual; EPFL: Lausanne, Switzerland, 2017; Available online: https://support.pix4d.com/hc/en-us/articles/204272989-Offline-Getting-Started-and-Manual-pdf (accessed on 30 July 2023).
71. Mesas-Carrascosa, F.J.; Torres-Sánchez, J.; Clavero-Rumbao, I.; García-Ferrer, A.; Peña, J.M.; Borra-Serrano, I.; López-Granados, F. Assessing Optimal Flight Parameters for Generating Accurate Multispectral Orthomosaicks by UAV to Support Site-Specific Crop Management. *Remote Sens.* **2015**, *7*, 12793–12814. [CrossRef]
72. Furukawa, Y.; Ponce, J. Accurate, Dense, and Robust Multiview Stereopsis. *IEEE Trans. Pattern Anal. Mach. Intell.* **2010**, *32*, 1362–1376. [CrossRef]
73. Khan, Z.; Rahimi-Eichi, V.; Haefele, S.; Garnett, T.; Miklavcic, S.J. Estimation of Vegetation Indices for High-Throughput Phenotyping of Wheat Using Aerial Imaging. *Plant Methods* **2018**, *14*, 20. [CrossRef]
74. Raeva, P.L.; Šedina, J.; Dlesk, A. Monitoring of Crop Fields Using Multispectral and Thermal Imagery from UAV. *Eur. J. Remote Sens.* **2019**, *52*, 192–201. [CrossRef]
75. Su, J.; Liu, C.; Chen, W.H. UAV Multispectral Remote Sensing for Yellow Rust Mapping: Opportunities and Challenges. *Unmanned Aer. Syst. Precis. Agric.* **2022**, *2*, 107–122. [CrossRef]
76. Yu, J.; Wang, J.; Leblon, B.; Song, Y. Nitrogen Estimation for Wheat Using UAV-Based and Satellite Multispectral Imagery, Topographic Metrics, Leaf Area Index, Plant Height, Soil Moisture, and Machine Learning Methods. *Nitrogen* **2021**, *3*, 1–25. [CrossRef]
77. Rouse, J.; Haas, R.; Schell, J.; Deering, D. Monitoring vegetation systems in the Great Plains with ERTS-1. In Proceedings of the Third Earth Resources Technology Satellite Symposium, Washington, DC, USA, 10–14 December 1974; pp. 309–317.
78. Rasmussen, C.E. *Gaussian Processes in Machine Learning*; Bousquet, O., Luxburg, U., Rätsch, G., Eds.; Springer: Berlin/Heidelberg, Germany, 2004; pp. 63–71. [CrossRef]
79. Rasmussen, C.E.; Williams, C.K. *Gaussian Processes for Machine Learning*; MIT Press: Cambridge, MA, USA, 2006.
80. Shi, J.Q.; Choi, T. *Gaussian Process Regression Analysis for Functional Data*; CRC Press: Boca Raton, FL, USA, 2011.
81. Camps-Valls, G.; Verrelst, J.; Munoz-Mari, J.; Laparra, V.; Mateo-Jimenez, F.; Gomez-Dans, J. A Survey on Gaussian Processes for Earth-Observation Data Analysis: A Comprehensive Investigation. *IEEE Geosci. Remote Sens. Mag.* **2016**, *4*, 58–78. [CrossRef]
82. Breiman, L. *Bagging Predictors*; Kluwer Academic Publishers: Dordrecht, The Netherlands, 1996; pp. 123–140.
83. Friedman, J.H. Greedy Function Approximation: A Gradient Boosting Machine. *Ann. Stat.* **2001**, *29*, 1189–1232. Available online: https://www.jstor.org/stable/2699986 (accessed on 2 September 2023). [CrossRef]
84. Quinlan, J.R. Bagging, boosting, and c4.5. In Proceedings of the Thirteenth National Conference on Artificial, Portland, Oregon, 4–8 August 1996.
85. Sun, J.; Yang, J.; Shi, S.; Chen, B.; Du, L.; Gong, W.; Song, S. Estimating Rice Leaf Nitrogen Concentration: Influence of Regression Algorithms Based on Passive and Active Leaf Reflectance. *Remote Sens.* **2017**, *9*, 951. [CrossRef]
86. Dietterich, T.G. *Ensemble Methods in Machine Learning. Multiple Classifier Systems*; Springer: Berlin/Heidelberg, Germany, 2000; pp. 1–15. [CrossRef]
87. Abu Al-Haija, Q.; Odeh, A.; Qattous, H. PDF Malware Detection Based on Optimizable Decision Trees. *Electronics* **2022**, *11*, 3142. [CrossRef]
88. Raza, A.; Ali, M.; Ehsan, M.K.; Sodhro, A.H. Spectrum Evaluation in CR-Based Smart Healthcare Systems Using Optimizable Tree Machine Learning Approach. *Sensors* **2023**, *23*, 7456. [CrossRef]
89. Cortes, C.; Vapnik, V. Support-Vector Networks. *Mach. Learn.* **1995**, *20*, 273–297. [CrossRef]
90. Pal, M. Kernel methods in remote sensing: A review. *ISH J. Hydraul. Eng.* **2009**, *15*, 194–215. [CrossRef]
91. Murty, M.N.; Raghava, R. *Support Vector Machines and Perceptrons: Learning, Optimization, Classification, and Application to Social Networks*, 1st ed.; Springer International Publishing: Berlin/Heidelberg, Germany, 2016.
92. Fan, R.E.; Chen, P.H.; Lin, C.J. Working set selection using second order information for training support vector machines. *J. Mach. Learn. Res.* **2005**, *6*, 1889–1918.
93. Kotsiantis, S.B.; Zaharakis, I.D.; Pintelas, P.E. Machine Learning: A Review of Classification and Combining Techniques. *Artif. Intell. Rev.* **2006**, *26*, 159–190. [CrossRef]
94. Ndikumana, E.; Ho Tong Minh, D.; Dang Nguyen, H.T.; Baghdadi, N.; Courault, D.; Hossard, L.; El Moussawi, I. Estimation of Rice Height and Biomass Using Multitemporal SAR Sentinel-1 for Camargue, Southern France. *Remote Sens.* **2018**, *10*, 1394. [CrossRef]
95. Obaido, G.; Ogbuokiri, B.; Swart, T.G.; Ayawei, N.; Kasongo, S.M.; Aruleba, K.; Esenogho, E. An Interpretable Machine Learning Approach for Hepatitis B Diagnosis. *Appl. Sci.* **2022**, *12*, 11127. [CrossRef]
96. Huang, T.; Kecman, V.; Kopriva, I. *Kernel Based Algorithms for Mining Huge Data Sets*; Springer: Berlin/Heidelberg, Germany, 2006; Volume 17. [CrossRef]
97. Deka, P.C. Support Vector Machine Applications in the Field of Hydrology: A Review. *Appl. Soft Comput.* **2014**, *19*, 372–386. [CrossRef]
98. Kleijnen, J.P. Kriging Metamodeling in Simulation: A Review. *Eur. J. Oper. Res.* **2009**, *192*, 707–716. [CrossRef]

99. Jena, R.K.; Bandyopadhyay, S.; Pradhan, U.K.; Moharana, P.C.; Kumar, N.; Sharma, G.K.; Hossain, A. Geospatial Modelling for Delineation of Crop Management Zones Using Local Terrain Attributes and Soil Properties. *Remote Sens.* **2022**, *14*, 2101. [CrossRef]
100. McBratney, A.B.; Webster, R. Choosing Functions for Semi-Variograms of Soil Properties and Fitting Them to Sampling Estimates. *J. Soil Sci.* **1986**, *37*, 617–639. [CrossRef]
101. Miller, M.P.; Singer, M.J.; Nielsen, D.R. Spatial Variability of Wheat Yield and Soil Properties on Complex Hills. *Soil Sci. Soc. Am. J.* **1988**, *52*, 1133–1141. [CrossRef]
102. Carslaw, D.C.; Ropkins, K. Openair—An R Package for Air Quality Data Analysis. *Environ. Model. Softw.* **2012**, *27–28*, 52–61. [CrossRef]
103. Xu, C.; Ding, Y.; Zheng, X.; Wang, Y.; Zhang, R.; Zhang, H.; Xie, Q. A Comprehensive Comparison of Machine Learning and Feature Selection Methods for Maize Biomass Estimation Using Sentinel-1 SAR, Sentinel-2 Vegetation Indices, and Biophysical Variables. *Remote Sens.* **2022**, *14*, 4083. [CrossRef]
104. Rashid, M.; Kanwal, S.; Ghafar, S.; Nawwal, K.; Ajmal, S.; Rasib, S. Assessment of Soil Texture on *Triticum aestivum* Growth. In Proceedings of the 1st International Conference on Energy, Power and Environment, Gujrat, Pakistan, 11–12 November 2021; p. 14. [CrossRef]
105. Cambardella, C.A.; Moorman, T.B.; Novak, J.M.; Parkin, T.B.; Karlen, D.L.; Turco, R.F.; Konopka, A.E. Field-Scale Variability of Soil Properties in Central Iowa Soils. *Soil Sci. Soc. Am. J.* **1994**, *58*, 1501–1511. [CrossRef]
106. Fernández, F.G.; Hoeft, R.G. Managing Soil PH and Crop Nutrients. In *Illinois Agronomy Handbook*; University of Illinois at Urbana Champaign: Champaign, IL, USA, 2009; p. 22.
107. Crema, A.; Boschetti, M.; Nutini, F.; Cillis, D.; Casa, R. Influence of Soil Properties on Maize and Wheat Nitrogen Status Assessment from Sentinel-2 Data. *Remote Sens.* **2020**, *12*, 2175. [CrossRef]
108. Wang, Q.; Chen, X.; Meng, H.; Miao, H.; Jiang, S.; Chang, Q. UAV Hyperspectral Data Combined with Machine Learning for Winter Wheat Canopy SPAD Values Estimation. *Remote Sens.* **2023**, *15*, 4658. [CrossRef]
109. Bian, C.; Shi, H.; Wu, S.; Zhang, K.; Wei, M.; Zhao, Y.; Chen, S. Prediction of Field-Scale Wheat Yield Using Machine Learning Method and Multi-Spectral UAV Data. *Remote Sens.* **2022**, *14*, 1474. [CrossRef]
110. Kravchenko, A.; Bullock, D.G. A Comparative Study of Interpolation Methods for Mapping Soil Properties. *Agron. J.* **1999**, *91*, 393–400. [CrossRef]
111. Zhu, Q.; Lin, H.S. Comparing Ordinary Kriging and Regression Kriging for Soil Properties in Contrasting Landscapes. *Pedosphere* **2010**, *20*, 594–606. [CrossRef]
112. Houlong, J.; Daibin, W.; Chen, X.; Shuduan, L.; Hongfeng, W.; Chao, Y.; Najia, L.; Yiyin, C.; Lina, G. Comparison of Kriging Interpolation Precision between Grid Sampling Scheme and Simple Random Sampling Scheme for Precision Agriculture. *Eurasian J. Soil Sci.* **2016**, *5*, 62. [CrossRef]
113. Goh, B.B.; King, P.; Whetton, R.L.; Sattari, S.Z.; Holden, N.M. Monitoring Winter Wheat Growth Performance at Sub-Field Scale Using Multitemporal Sentinel-2 Imagery. *Int. J. Appl. Earth Obs. Geoinf.* **2022**, *115*, 103124. [CrossRef]
114. Jachowski, N.R.A.; Quak, M.S.Y.; Friess, D.A.; Duangnamon, D.; Webb, E.L.; Ziegler, A.D. Mangrove Biomass Estimation in Southwest Thailand Using Machine Learning. *Appl. Geogr.* **2013**, *45*, 311–321. [CrossRef]
115. Ghosh, S.S.; Dey, S.; Bhogapurapu, N.; Homayouni, S.; Bhattacharya, A.; McNairn, H. Gaussian Process Regression Model for Crop Biophysical Parameter Retrieval from Multi-Polarized C-Band SAR Data. *Remote Sens.* **2022**, *14*, 934. [CrossRef]
116. Verrelst, J.; Alonso, L.; Camps-Valls, G.; Delegido, J.; Moreno, J. Retrieval of Vegetation Biophysical Parameters Using Gaussian Process Techniques. *IEEE Trans. Geosci. Remote Sens.* **2012**, *50*, 1832–1843. [CrossRef]
117. Gewali, U.B.; Monteiro, S.T.; Saber, E. Gaussian Processes for Vegetation Parameter Estimation from Hyperspectral Data with Limited Ground Truth. *Remote Sens.* **2019**, *11*, 1614. [CrossRef]
118. Roy Choudhury, M.; Das, S.; Christopher, J.; Apan, A.; Chapman, S.; Menzies, N.W.; Dang, Y.P. Improving Biomass and Grain Yield Prediction of Wheat Genotypes on Sodic Soil Using Integrated High-Resolution Multispectral, Hyperspectral, 3D Point Cloud, and Machine Learning Techniques. *Remote Sens.* **2021**, *13*, 3482. [CrossRef]
119. Lin, X.; Shang, R.; Chen, J.M.; Zhao, G.; Zhang, X.; Huang, Y.; Jiao, W. High-Resolution Forest Age Mapping Based on Forest Height Maps Derived from GEDI and ICESat-2 Space-Borne Lidar Data. *Agric. For. Meteorol.* **2023**, *339*, 109592. [CrossRef]
120. Jiang, X.; Fang, S.; Huang, X.; Liu, Y.; Guo, L. Rice Mapping and Growth Monitoring Based on Time Series GF-6 Images and Red-Edge Bands. *Remote Sens.* **2021**, *13*, 579. [CrossRef]
121. John, K.; Abraham Isong, I.; Michael Kebonye, N.; Okon Ayito, E.; Chapman Agyeman, P.; Marcus Afu, S. Using Machine Learning Algorithms to Estimate Soil Organic Carbon Variability with Environmental Variables and Soil Nutrient Indicators in an Alluvial Soil. *Land* **2020**, *9*, 487. [CrossRef]